The Coupling of Upper and Lower Tropospheric Jet Streaks and Implications for the Development of Severe Convective Storms

LOUIS W. UCCELLINI[1]

Space Science and Engineering Center, University of Wisconsin, Madison 53706

DONALD R. JOHNSON

Space Science and Engineering Center and Department of Meteorology, University of Wisconsin, Madison 53706

(Manuscript received 17 July 1978, in final form 2 March 1979)

ABSTRACT

Transverse circulations in the exit and entrance regions of jet streaks are investigated through numerical simulation, a case study, and an application of the isallobaric wind equation in isentropic coordinates, to study the interaction between upper and lower tropospheric jets and the development of severe convective storms. A hybrid isentropic-sigma coordinate numerical model is used to simulate the mass and momentum adjustments associated with a jet streak propagating in a zonal channel. The numerical results depict a two-layer mass adjustment in the exit and entrance region of the jet streak. The results also verify that the isallobaric wind on lower isentropic surfaces is a primary component of the return branches of transverse circulations and is forced by the two-layer mass adjustment accompanying the propagating jet streak. Results from the case study of a severe weather outbreak show that 1) a low-level jet (LLJ) beneath the exit region of an upper tropospheric jet streak is embedded in the lower branch of an indirect circulation, 2) intensification of the lower branch and development of the LLJ is largely a result of an increased isallobaric wind component, and 3) the development of the LLJ is coupled to the upper tropospheric jet streak by the two-layer mass adjustment within the exit region of the streak. The isallobaric wind component of the LLJ is the primary reason for the axis of the LLJ being at a significant angle to the upper jet's axis and the resulting veering of the wind with height. In the exit region, the geometry of this adjustment, combined with warm, moist, lower tropospheric air to the right and ahead of the jet streak and cool, dry air at the jet streak level, produced the differential advections that convectively destabilized the atmosphere. Results of the case study support the concept that the development of conditions favorable for severe convective storms can be forced by mass and momentum adjustments which accompany the propagation of an upper tropospheric jet streak.

1. Introduction

The concept that an interaction between upper and lower trophospheric jet streaks is important for the development of organized convective storm systems was implied in the work of Fawbush and Miller (1953, 1954). They noted that advection of cool, dry air associated with strong westerly winds in the middle troposphere and the rapid northward movement of a tongue of warm, moist air in the low troposphere create favorable conditions for deep convection. They also emphasized that the likelihood of convection is increased with strong veering of winds, so that the angle between the mid-tropospheric wind and the axis of the moisture tongue is large. Petterssen (1956) and Newton (1967), among others, related veering of winds with height and subsequent differential moisture and temperature advections to the intersection of jet axes (Fig. 1) and the development of convective instability. The greatest convective instability develops when the jet axes tend to be orthogonal and the intensity of the advections is maximized.

The roles of tropospheric jet streaks[2] in the development of severe convective storms are summarized by Petterssen (1956), Reiter (1963), Ludlam (1963), Newton (1963, 1967), Palmén and Newton (1969) and Danielsen (1974). In these models the primary role of the upper trophospheric jet streak is to advect cool, dry air within the upper and middle troposphere, to enhance upper level divergence, and to transport the sensible heat downstream from the convective region. The low-level jet (LLJ) rapidly transports heat and moisture toward the convective region (see also Means, 1952, 1954; Bonner, 1966). The combined

[1] Present affiliation: NASA/Goddard Space Flight Center, Laboratory for Atmospheric Sciences, code 914, Greenbelt, MD 20771.

[2] Palmén and Newton (1969, p. 199) define jet streaks as the regions of isotach maxima.

0027-0644/79/060682-22$09.50

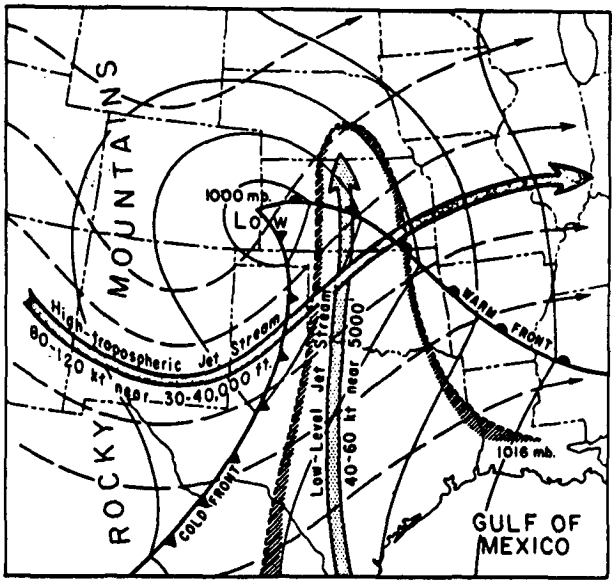

FIG. 1. Schematic features of a severe weather outbreak. Solid lines are sea level isobars; dashed lines streamlines of upper tropospheric flow. Shading outlines general area of low-level moisture tongue and region of potential instability (from Newton, 1967).

role of the upper and lower trophospheric jet streaks is to create a region of convective instability within which the severe weather ultimately occurs. Beebe and Bates (1955) also related the relative orientation and position of the two jets to a superposition of divergent and convergent fields which induces mechanical lifting and initiates the convective storms. Reiter (1963) offered additional evidence of vorticity advection, divergence and vertical exchange of momentum in his emphasis that jet streaks exert a causal mechanism in the production of severe weather, while Ludlam (1963) showed that the mean position of the jet streak is closely related to the global distribution of severe convection.

With the analyses of upper and lower tropospheric jet streaks normally depicted on pressure surfaces, these jets are normally treated as separate entities in the criteria for the development of severe convective storms. However, with jet streaks analyzed on isentropic surfaces, the two apparently distinct jets appear to merge in some cases as the LLJ extends toward the middle troposphere (Reiter, 1969). Reiter suggested that, in some cases, low-level jets are not separate entities but appear to be coupled to an upper tropospheric jet streak.

The purposes of this study are to determine how upper and lower tropospheric jet streaks are coupled and to discuss the role of this coupling in the development of severe convective storms. In Section 2, types of low-level jet streaks which affect the North American continent are discussed and the type of LLJ selected for study is specified. The basis for coupling lower and upper tropospheric jet streaks that stems from adjustment concepts is presented in Section 3. A case study is discussed in Section 4 which links mass and momentum adjustments in the exit region of an upper tropospheric jet streak to the development of a LLJ and to the differential temperature and moisture transports that create favorable conditions for severe convective storms. A summary of the results and suggestions for future research is presented in Section 5.

2. Low-level jet streaks

Bonner's (1968) climatological summary illustrated the large number of lower tropospheric jet streaks that develop in the Great Plains and Midwest, with the maximum number of LLJ's occurring from Texas to Nebraska during the spring and summer months. The low-level jets in the southern Great Plains are characterized by a diurnal oscillation reaching maximum intensity by early morning, and are associated with a nocturnal temperature inversion (Blackadar, 1957; Wexler, 1961; Gerhardt, 1962, 1963; Hoecker, 1963; Izumi and Barad, 1963; Izumi, 1964; Bonner, 1968; Lettau, 1967). The seasonal shift of the subtropical high, sloped terrain, boundary-layer processes and the diurnal radiation cycle have all been related to the generation of the low-level jet and its seasonal, temporal and geographic preferences (Blackadar, 1957; Wexler, 1961; Lettau, 1967; Paegle and Rasch, 1973).

Reiter (1969) noted that lower tropospheric wind maxima also occur in the Midwest which appear to develop in response to synoptic or subsynoptic-scale forcing. Hoecker (1963) and Bonner (1966) presented examples of LLJ's in which lee side troughing or cyclogenesis is evident just east of the Rocky Mountains. These LLJ's developed with a minimal diurnal oscillation and extended above the planetary boundary layer to the 850 mb level. For similar cases, Danielsen (1974) pointed out that moisture-laden low-level wind maxima form in response to the increasing pressure gradients associated with the developing lee side cyclone. Supporting evidence for the existence of low-level jets in conjunction with cyclone evolution is presented in Browning and Harrold's (1970) Doppler radar observations of a cold front traversing the British Isles. They determined that prefrontal horizontal moisture transport is confined to the lower troposphere and is predominantly related to the lower tropospheric wind maximum located immediately ahead of and parallel to the cold front. This study is focused on synoptic-scale adjustments associated with the LLJ located beneath the exit region of the upper tropospheric jet streak, directed from the anticyclonic (south) toward the cyclonic (north) side (Fig. 1).

3. Mass and momentum adjustments associated with jet streaks

The mutual mass and momentum adjustments associated with a jet streak and the response of the lower tropospheric winds are discussed in this section. Since the LLJ located beneath the exit region of an upper tropospheric jet streak in severe weather situations is directed toward the cyclonic side of the jet (see Fig. 1), it would appear to be embedded within the return branch of the indirect circulation. Thus, isolating the forcing of a return branch of a transverse circulation through mass adjustment associated with a propagating wind maximum should provide insight into the coupling of upper and lower tropospheric jets.

Direct and indirect transverse circulations exist in entrance and exit regions of propagating jet streaks (University of Chicago, 1947; Namias and Clapp, 1949; Bjerknes, 1951; Riehl *et al.*, 1952; Murray and Daniels, 1953; Sawyer, 1956; Newton, 1959; Staley, 1960; Reiter, 1969; Johnson, 1970; Cahir, 1971; Uccellini, 1976). The indirect circulation within the exit region consists of an upper tropospheric branch directed toward the anticyclonic side of a jet, rising and sinking motion on the cyclonic and anticyclonic sides, respectively, and a lower tropospheric return branch directed toward the cyclonic side. The direct circulation in the entrance region is completely reversed from the sense of the indirect circulation.

The requirement that direct and indirect circulations must exist for unbalanced currents implicitly stems from the work of Rossby (1938, 1949), Cahn (1945) and Sawyer (1956). In a recent study of transverse circulations and subsynoptic precipitation bands, Cahir (1971) simulated direct and indirect circulations using a two-dimensional primitive equation model mapped on a vertical plane normal to a propagating jet streak and by applying the model to actual case studies. An example from Cahir's numerical simulation of an indirect circulation (Fig. 2) depicts upper and lower transverse components of 5.8 and 4.7 m s^{-1}, respectively, and vertical motions >2.0 μb s^{-1}. In a later experiment, with the initial relative humidities increased by 30%, the added latent heat release nearly doubled the magnitude of the upward vertical motion on the cyclonic side of the jet. Cahir applied his model to numerous cases and emphasized that subsynoptic-scale precipitation bands result from the upward vertical branches of both direct and indirect circulations associated with propagating jet streaks.

The verification of the transverse circulation from observational evidence is compounded by three-dimensional wave structure with its nonlinear advection associated with alongstream variation of momentum and pressure forces, stratification of the atmosphere, the influence of terrain, curvature effects, and interactions with large-scale waves during cyclone development and long-wave amplification (Newton, 1954; Beebe and Bates, 1955; Shapiro, 1975). Some three-dimensional aspects of mutual mass and momentum adjustments and coupling between the upper and lower troposphere will be identified in this paper through the geostrophic momentum approximation within an isentropic framework,

$$\frac{d\mathbf{U}}{dt} \approx \frac{d\mathbf{U}_g}{dt} \approx \frac{\partial \mathbf{U}_g}{\partial t_\theta} + \mathbf{U}\cdot\nabla_\theta \mathbf{U}_g + \frac{d\theta}{dt}\frac{\partial \mathbf{U}_g}{\partial \theta}, \quad (1)$$

where $\mathbf{U}$ and $\mathbf{U}_g$ are the horizontal and geostrophic winds, respectively (see Eliassen, 1949, 1962; Hoskins, 1975). With the relationship between horizontal acceleration and ageostrophic flow ($\mathbf{U}_{ag}$) expressed by

$$\mathbf{U}_{ag} = \mathbf{U} - \mathbf{U}_g = f^{-1}\mathbf{k} \times \frac{d\mathbf{U}}{dt}, \quad (2)$$

combined with the assumption of adiabatic flow and neglect of $(\mathbf{U}\cdot\nabla_\theta\mathbf{k}) \times \mathbf{U}_g$, an alternative form for the ageostrophic velocity is

$$\mathbf{U}_{ag} = f^{-1}\Big[\underbrace{\mathbf{k} \times \frac{\partial \mathbf{U}_g}{\partial t_\theta}}_{\text{A}} + \underbrace{\mathbf{U}\cdot\nabla_\theta(\mathbf{k} \times \mathbf{U}_g)}_{\text{B}}\Big]. \quad (3)$$

Term A represents the isallobaric wind (Brunt and Douglas, 1928), while term B accounts for advective, inertial processes. A quasi-geostrophic form of (3) is

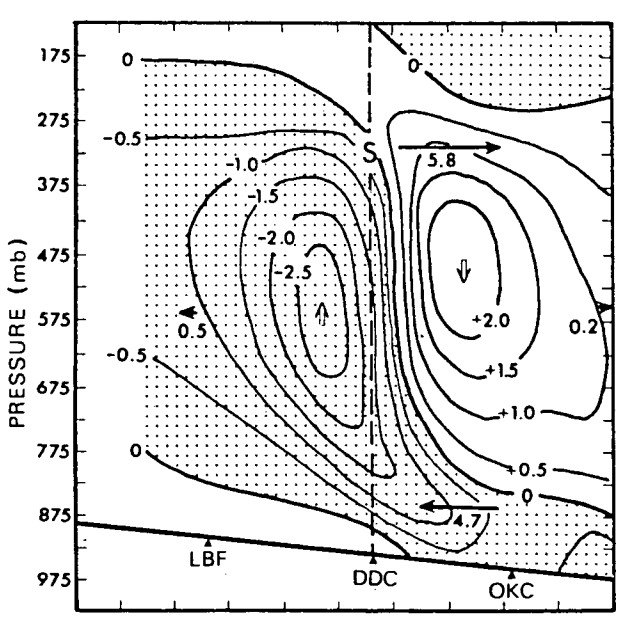

FIG. 2. Indirect circulation simulated by PE model mapped on cross section through exit region of a jet streak. Solid isopleths are vertical motion (μb s^{-1}) with upward motion stippled; arrows with centered magnitudes indicate horizontal transverse components (m s^{-1}) (from Cahir, 1971).

given by substituting $\mathbf{U}_g$ for the advecting velocity $\mathbf{U}$. However, including the ageostrophic component in term B yields significant differences in the quantitative assessment of advective processes in the regions of strong gradients near fronts and jet streaks (Hoskins, 1975). Note also that with the use of the adiabatic constraint within the isentropic framework, the link between the ageostrophic motion and inertial processes is solely by the quasi-horizontal advection. If the expansion of the total derivative were made in Cartesian or isobaric coordinates, term B would include a mode for upper and lower tropospheric interaction through vertical advection.

Using isentropic coordinates, an explicit isallobaric mode (term A) may be isolated to identify the interaction between the upper and lower troposphere through mass and momentum adjustments. Substituting the hydrostatic geostrophic relation

$$\mathbf{U}_g = f^{-1}\mathbf{k} \times \nabla_\theta \psi \tag{4}$$

in (3), the isallobaric component of the ageostrophic wind is

$$\mathbf{U}_{ag_i} = -f^{-2}\nabla_\theta \frac{\partial \psi}{\partial t_\theta}, \tag{5}$$

where ψ is the Montgomery streamfunction. Integration of the hydrostatic equation from the earth's surface to an intermediate isentropic surface θ_L yields

$$\psi_L = \psi_s + \int_{\theta_s}^{\theta_L} c_p \left(\frac{p}{p_{00}}\right)^{\kappa} d\theta, \tag{6}$$

where p is pressure, $p_{00} = 1000$ mb, and κ is the ratio of the gas constant R for dry air to the specific heat of constant pressure c_p. By Leibniz's rule, the local derivative of (6) is

$$\frac{\partial \psi_L}{\partial t_\theta} = \frac{\partial \psi_s}{\partial t_\theta} + \frac{c_p \kappa}{p_{00}} \int_{\theta_s}^{\theta_L} \left(\frac{p}{p_{00}}\right)^{\kappa-1} \frac{\partial p}{\partial t_\theta} d\theta - c_p \left(\frac{p_s}{p_{00}}\right)^{\kappa} \frac{\partial \theta_s}{\partial t_\theta}. \tag{7}$$

With Poisson's equation and the definition of ψ, the time derivative of the surface value of the Montgomery streamfunction is

$$\frac{\partial \psi_s}{\partial t_\theta} = c_p \left(\frac{p_s}{p_{00}}\right)^{\kappa} \frac{\partial \theta_s}{\partial t_\theta} + \frac{c_p \theta_s \kappa}{p_{00}} \left(\frac{p_s}{p_{00}}\right)^{\kappa-1} \frac{\partial p_s}{\partial t_\theta}. \tag{8}$$

Substitution of (8) into (7) and a rearrangement of terms yields

$$\frac{\partial \psi_L}{\partial t_\theta} = R\left[\frac{T_s}{p_s}\frac{\partial p_s}{\partial t_\theta} + \int_{\theta_s}^{\theta_L} \left(\frac{p}{p_{00}}\right)^{\kappa} \frac{1}{p}\frac{\partial p}{\partial t_\theta} d\theta\right]. \tag{9}$$

With this result and (5), the isallobaric component of the ageostrophic wind ($\mathbf{U}_{ag_i}$) on θ_L is

$$\mathbf{U}_{ag_i}(\theta_L) = -\frac{R}{f^2}\left\{\nabla\left[\frac{T_s}{p_s}\frac{\partial p_s}{\partial t_\theta}\right] + \nabla\left[\int_{\theta_s}^{\theta_L} \left(\frac{p}{p_{00}}\right)^{\kappa} \frac{1}{p}\frac{\partial p}{\partial t_\theta} d\theta\right]\right\}. \tag{10}$$

The form of (10) reveals that the isallobaric wind in isentropic coordinates is determined by the gradients of the surface pressure tendency and the integrated pressure tendency between the earth's surface and θ_L. In a hydrostatic atmosphere, the tendency of the vertically integrated mass distribution determines the first term, while the second term is related to internal mass redistribution. Note that the isallobaric wind component may exist on an isentropic surface even if the surface pressure tendency is zero.

The relationship between the pressure tendencies and $\mathbf{U}_{ag_i}$ expressed in (10) couples tropospheric mass adjustment to the isallobaric wind on θ_L. The vertical integration of the mass continuity equation between arbitrary lower and upper isentropic surfaces (θ_2 and θ_1) yields

$$\frac{\partial p_2}{\partial t_\theta} = \frac{\partial p_1}{\partial t_\theta} + \int_{\theta_2}^{\theta_1} \left[\nabla_\theta \cdot \frac{\partial p}{\partial \theta}\mathbf{U} + \frac{\partial}{\partial \theta}\left(\frac{\partial p}{\partial \theta}\frac{d\theta}{dt}\right)\right] d\theta. \tag{11}$$

With the substitution of (11) into (10), the isallobaric ageostrophic component on θ_L can be linked to horizontal mass divergence and diabatic processes.

a. Mass adjustments associated with a propagating jet streak

The results from a hybrid isentropic and sigma coordinate numerical model are used to illustrate mass-momentum adjustments associated with the jet streak's propagation in a zonal channel. Following is a brief summary of the hybrid model described in detail by Uccellini *et al.* (1979). The hybrid model combines an isentropic representation of the free atmosphere with a sigma coordinate representation of the bottom 200 mb of the troposphere. The boundary conditions at the interface separating the model domains are matched exactly through use of the flux form of the governing equations for full interaction between the model domains without introducing spurious sources of mass, momentum and energy. A staggered vertical grid is used to maintain a smooth transition of the mass and wind fields without need for artificial adjustments. The longitudinal boundary conditions are cyclic while impervious, free-slip conditions are imposed on the latitudinal boundaries. The initial mass field is specified by a set of analytic functions which define the surface temperature gradient and the vertical lapse rates throughout the

entire model domain. The initial wind field is specified through the geostrophic relationship.

Areal average mass flux divergence was calculated for a $4\Delta x$ by $3\Delta y$ rectangle ($\Delta x = \Delta y = 2.75 \times 10^5$ m) in each of the four quadrants surrounding the jet streak 16 h into the model simulation. The averages were computed for the eight layers between 290 and 350 K with $\Delta\theta$ equal to 10 K.

With adiabatic conditions, the mass flux divergence is related solely to the horizontal mass flux divergence term in (11). The vertical distribution of the averaged total mass flux divergence (solid profile) illustrates a two-layer mass adjustment in the entrance and exit regions of the jet streak (Fig. 3). In the cyclonic exit and anticyclonic entrance quadrants, the upper tropospheric mass divergence is complemented by lower tropospheric mass convergence with the level of nondivergence located near 310 K. A reverse pattern exists in the anticyclonic exit and cyclonic entrance regions. The four-cell, two-layer pattern is consistent with Bjerknes' (1951) and Riehl *et al.* (1952) concepts of adjustments associated with a jet streak.

Some indication of the relative importance of geostrophic versus ageostrophic motion at this scale may be determined by partitioning the mass flux diver-

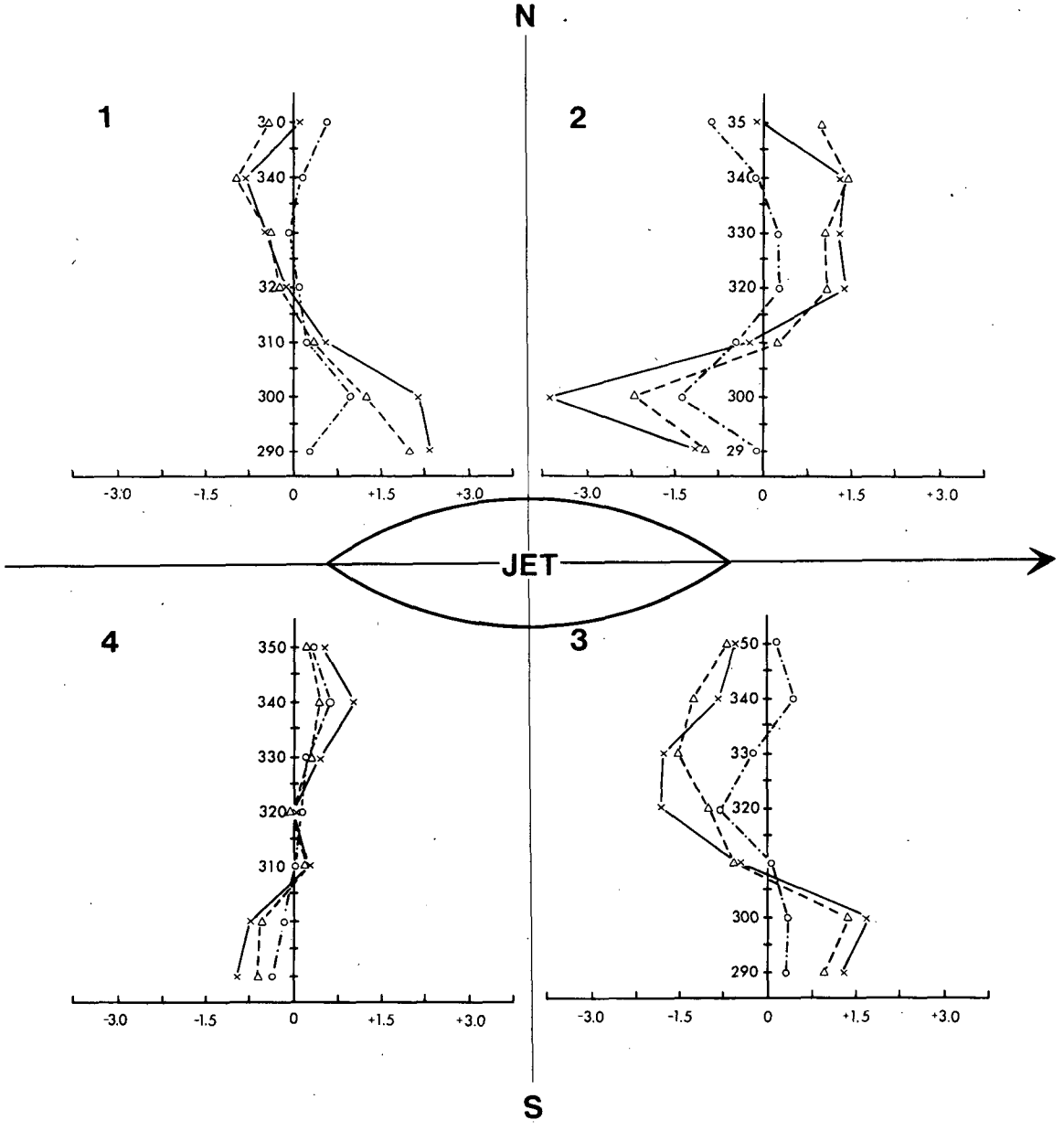

FIG. 3. Modeled vertical profiles for the averaged mass flux divergence ($\times 10^1$ g m^{-2} s^{-1}) [total (solid), ageostrophic (dashed), geostrophic (dot-dashed)] in four quadrants surrounding jet streak.

gence into a geostrophic and ageostrophic mode, where

$$\nabla_\theta\cdot(\rho J\mathbf{U}) = \nabla_\theta\cdot(\rho J\mathbf{U}_g) + \nabla_\theta\cdot(\rho J\mathbf{U}_{ag}), \quad (12)$$

where ρJ (density; Jacobian of transformation) is equal to $-(1/g)\partial p/\partial\theta$. The relative amplitude of the geostrophic (dot-dashed profile) versus the ageostrophic mode (dashed profile) shows that the ageostrophic mode of the mass flux divergence dominates at this scale of the mass adjustment (Fig. 3).

b. The upper tropospheric transverse component

An analysis of the components of the ageostrophic mass flux divergence (not shown) reveals that the cross-stream component $\partial(\rho J v_{ag})/\partial y$ generally dominates in the lower troposphere. In the upper troposphere, the cross-stream and alongstream ageostrophic components are of equal magnitude and of the same sign. Bjerknes (1951) emphasized the need for upper tropospheric ageostrophic components to provide for the cross-stream mass transport in the exit and entrance regions of the jet streak. In the exit region, the upper tropospheric, ageostrophic wind transports mass from the cyclonic toward the anticyclonic side of the jet. In the entrance region, the upper tropospheric ageostrophic wind transports mass from the anticyclonic toward the cyclonic side of the jet. At the level of the jet streak, where the horizontal variations of the pressure gradient force and wind are maximized, the advective inertial term in (3) tends to be larger than and offsets the isallobaric term in the forcing of a transverse ageostrophic component (Bjerknes, 1951). Fig. 4 illustrates the 340 K ageostrophic wind component defined by the inertial advective term. In the entrance region, the increase of the geostrophic wind along the direction of the streak yields a maximum ageostrophic transverse wind component of 4.5 m s^{-1} directed toward the cyclonic side. In the exit region, the decrease in the geostrophic wind along the axis of the jet yields a maximum ageostrophic transverse wind component of 8.5 m s^{-1} directed toward the anticyclonic side. This basic pattern propagates with the jet streak and remains quasi-steady.

c. The lower tropospheric return branch viewed as an isallobaric wind component

The opposite pattern of the areal average mass flux divergence below the 310 K level in each quadrant (Fig. 3) is an indication of the reversal of the lower tropospheric branches of the direct and indirect circulations from the upper branches illustrated in Fig. 4. In the lower troposphere, where advective velocities are small and inertia wind components are strongly damped by friction, the isallobaric wind modified by friction becomes a more important factor for low-level parcel accelerations and resultant ageostrophic flow (Hess, 1959; Young, 1973). In comparing the two contributing terms to $\mathbf{U}_{ag}$ in (3), the isallobaric wind (term A) is the dominant factor of the lower tropospheric transverse ageostrophic wind component for this model simulation. The largest, lower tropospheric isallobaric wind components are perpendicular to the axis of the jet streak and are opposite in direction to the inertial advective component of the upper branches (Fig. 5).

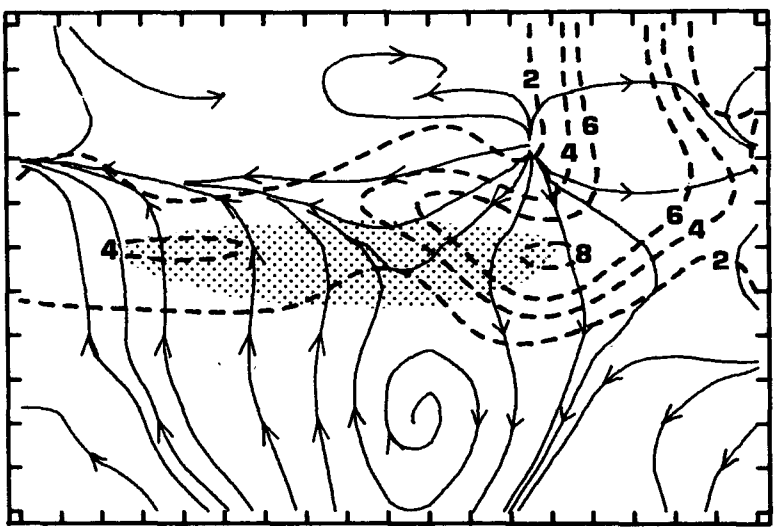

FIG. 4. Model simulated ageostrophic component related to the inertial-advective term [term B, Eq. (3)] on the 340 K surface. Streamline analysis (solid lines) is shown for the model domain up to the first interior row of grid points along the north and south boundaries; magnitudes (m s^{-1}) are shown as dashed lines. Shaded region represents jet streak (u component >40 m s^{-1}). The marks along the border represent 275 km grid spacing.

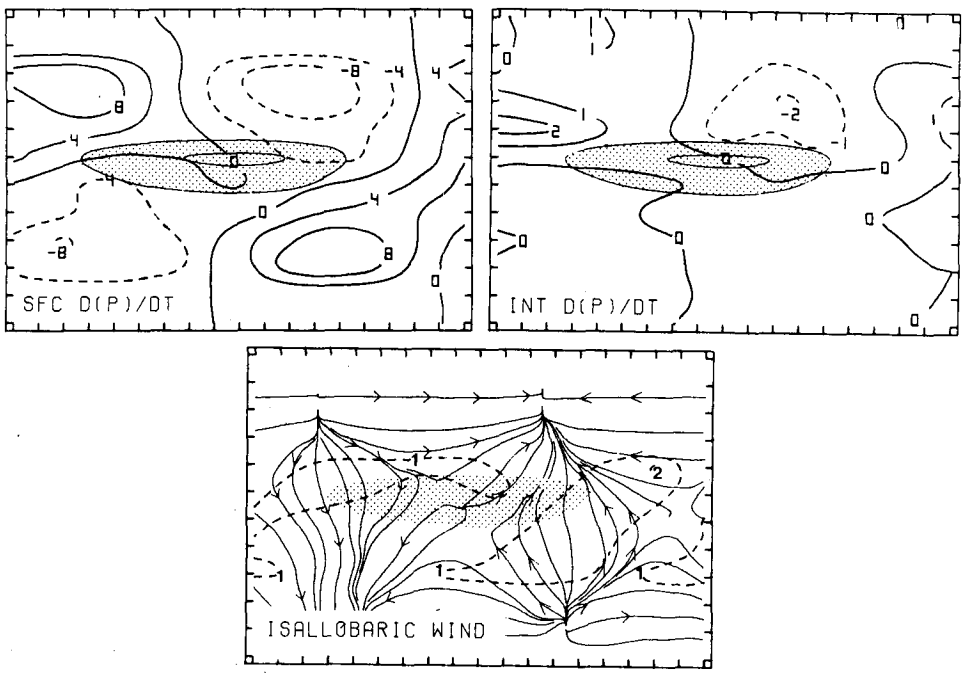

FIG. 5. (Above) The surface pressure tendency and integrated pressure tendency contributions to the ψ tendency from (9) evaluated on 300 K ($\times 10^{-3}$ m^2 s^{-3}). (Below) Streamline analysis is shown for isallobaric wind with magnitudes (m s^{-1}) as dashed line. See caption in Fig. 4 for additional details.

Maximum values of 1.5 m s^{-1} are located immediately ahead of and behind the streak. This basic pattern of the isallobaric wind components propagates with the jet streak and also remains quasi-steady at subsequent times.

Fig. 5 also illustrates the relation of the isallobaric wind to mass adjustments within the exit and entrance regions of the upper tropospheric jet streak. The surface and integrated pressure tendency terms in (9) were evaluated with θ_L equal to 300 K to determine the forcing of the isallobaric component within the return branches. Both terms display the basic four-cell pattern, with the surface pressure tendency term noticeably larger in these adiabatic experiments. In the cyclonic exit and anticyclonic entrance regions, pressure tendencies are negative while positive tendencies exist in the anticyclonic exit and cyclonic entrance regions. As specified by (10), the patterns of both pressure tendencies act to force the isallobaric wind directed toward the cyclonic and anticyclonic sides of the jet streak beneath the exit and entrance regions. These ageostrophic, isallobaric wind components represent lower tropospheric return branches of direct and indirect circulations.

d. Coupling the transverse branches to tropospheric mass adjustment

The principal components of the upper and lower tropospheric branches of the direct and indirect circulation are summarized in Fig. 6. In the entrance region of the upper tropospheric jet, confluent streamlines and downwind increase of the geostrophic wind are linked with the inertial advective process and are associated with a transverse ageostrophic component directed toward the cyclonic side of the jet streak (Fig. 6A). In the exit region, diffluent streamlines and a downwind decrease of the geostrophic wind are associated with an ageostrophic component directed towards the anticyclonic side. The upper tropospheric, cross-stream mass transports that are a result of the transverse components act to force the lower tropospheric isallobaric winds which represent the lower branches of the transverse circulations. Beneath the entrance region of the upper tropospheric jet streak, the upper tropospheric mass transport reduces the slope of the lower tropospheric isentropic surface (as p increases to the left and decreases to the right), decreases the ψ gradient, and yields an ageostrophic component on θ_L directed to the right of the current (Fig. 6B). Beneath the exit region, the upper tropospheric mass transport increases the slope of the isentropic surface and the ψ gradient to yield an ageostrophic component on θ_L directed to the left of the current (Fig. 6C). These ageostrophic components in the upper and lower troposphere represent the *transverse components* of the direct and indirect circulations, while the total wind component (U in Fig. 6) represents the *total* upper and lower tropospheric branches of the circulations.

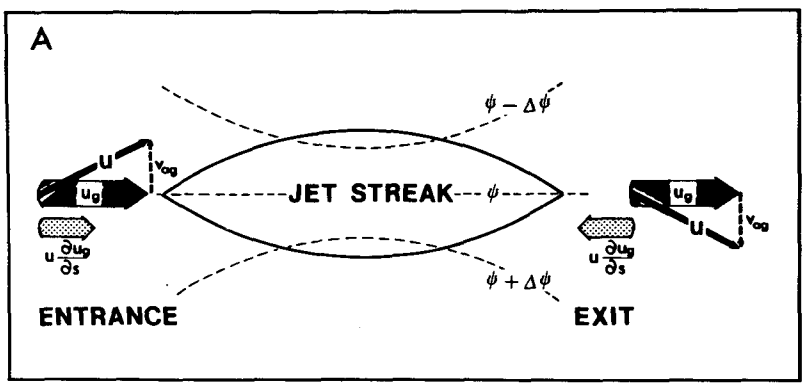

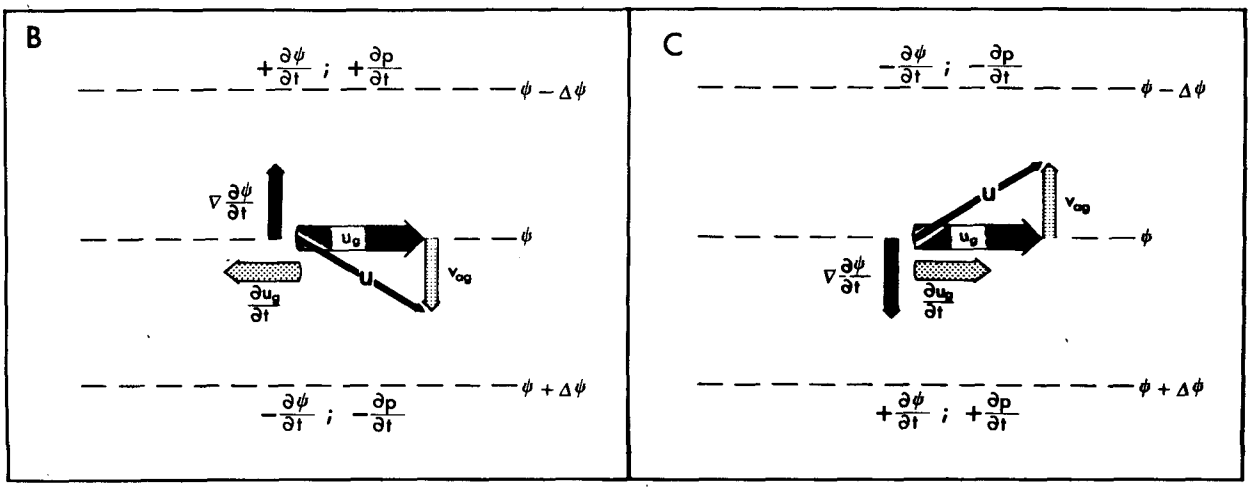

FIG. 6. (A) Schematic of transverse component (v_{ag}) forced by along-stream variations of pressure gradient force at jet streak level. (B), (C) Isallobaric wind (v_{ag}) on lower tropospheric isentropic surface (θ_L) beneath the entrance (B) and exit (C) regions of the jet streak. Geostrophic wind is U_g, total wind is U, pressure is p and the alongstream coordinate is s.

The schematic in Fig. 7 depicts a cross-sectional view of the lower tropospheric isallobaric wind forced by adiabatic mass adjustments in the exit region of a jet streak. As a jet streak (J) propagates toward the vertical cross section in Fig. 7A, the upper tropospheric ageostrophic component transports mass toward the anticyclonic side of the jet. The mass flux convergence on the anticyclonic side and divergence on the cyclonic side above θ_L increases the pressure on and beneath θ_L to the right of the jet, and decreases the pressure to the left of the jet. By (9) the mass adjustment within the upper branches above θ_L increases the magnitude of the pressure gradient force on and beneath θ_L and by (10) concurrently forces development of an isallobaric wind that represents a return branch of the indirect circulation (Fig. 7B). With the concurrent development of the return branch, mass is transported toward the cyclonic side of the jet below θ_L. This response represents a mutual mass-momentum adjustment and is an integral part of the sinking and lifting of isentropic surfaces beneath θ_L to higher and lower pressures on the anticyclonic and cyclonic sides of the jet, respectively. The two-layer adjustment depicted in Fig. 7 stems from Rossby's adjustment concepts for a stratified fluid (Rossby, 1938, 1949; University of Chicago, 1947).

A schematic of the influence of cross-stream variation of diabatic mass transport in increasing the magnitude of the pressure gradient on θ_L is depicted in Figs. 7C and 7D. An increase in the isallobaric wind on θ_L will occur with either diabatic heating to the right or diabatic cooling to the left. The heating vertically transports mass from below to above θ_L, while cooling transports mass from above θ_L to below θ_L

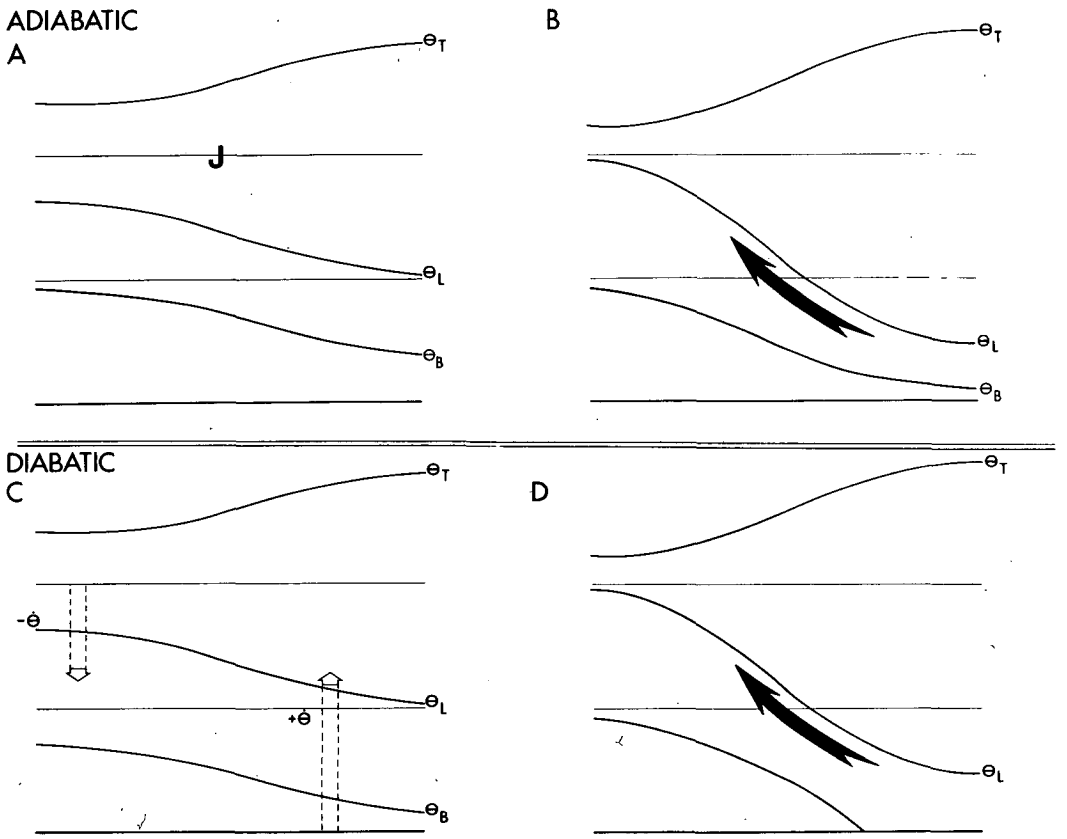

FIG. 7. (A), (B) Vertical cross section normal to axis of jet (J) showing adiabatic mass transports in exit region of approaching jet streak and resultant isallobaric wind (heavy arrow in B). (C), (D) Diabatic mass transports contributing to isallobaric wind (heavy arrow in D).

(Fig. 7C). Since diabatic mass transports are vertical, the surface pressure tendencies are not directly affected by the first term in (9) which reduces to zero. However, with the assumed diabatic mass transports depicted in Fig. 7C the vertically integrated pressure tendency term in (9) becomes positive to the right and negative to the left for isentropic surfaces below θ_L. As a consequence, the intensification of the pressure gradient force generates a diabatic component of the isallobaric wind along θ_L, directed toward the left (Fig. 7D). It is likely that the release of latent energy *may at times* force such a component if the cumulus convection develops in warm moist regions to the right of the jet streak. The diabatic mass transport related to sensible heat flux could also be important as θ_L approaches the planetary boundary layer to the right of the jet. If the diabatic heating is maximized to the left of the jet, as is implied by Fig. 1, the magnitude of the isallobaric component would be reduced. Since the preliminary model experiments were for a dry atmosphere, these effects could not be evaluated to determine their relative importance.

4. Case study: 10–11 May 1973

Evidence of coupling between upper and lower tropospheric jet streaks by mutual mass-momentum adjustments and the subsequent generation of convective instability is now presented from a case study. The severe weather outbreak over Indiana and Ohio on 10–11 May 1973 was selected for study since the lack of cyclogenesis in this case allows for the isolation of mass adjustments and the response of the lower tropospheric wind forced primarily by a jet streak.

The synoptic conditions preceding the development of the severe convective storms are described in this section. The propagation of an upper tropospheric jet streak and two-layered mass adjustment are studied to establish the forcing of the lower tropospheric isallobaric wind on the 300 K surface. A diagnostic trajectory analysis is then applied to link the isallobaric wind and the development of a low-level jet on the 300 K surface. Finally, the development of the LLJ and its interaction with the upper tropospheric jet streak are related to the development of the convective storm system in eastern Indiana and Ohio.

a. Surface and radar analyses

On the morning (1200 GMT) of 10 May 1973, a diffuse low-pressure system was located in the Great Lakes and Hudson Bay regions with a weak cold

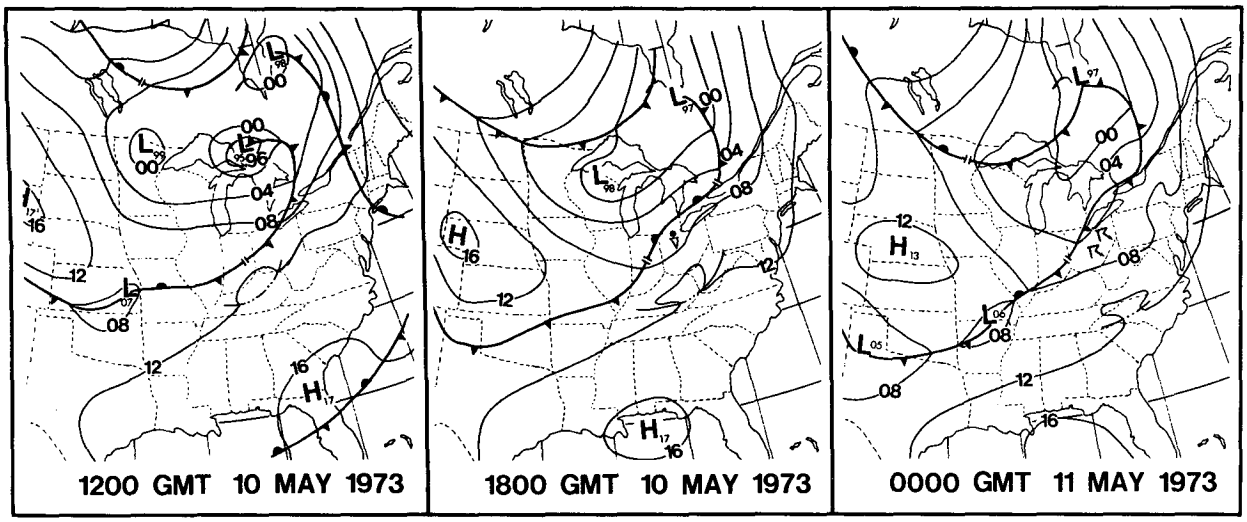

FIG. 8. Surface isobar analyses (mb, 08 = 1008 mb) for 1200 GMT 10 May through 0000 GMT 11 May 1973.

front extending from east of Lake Huron southwestward through southern Illinois and Missouri where a stationary front connected to a weak low in Kansas (Fig. 8). At 1800 GMT 10 May, the low in the Great Lakes region remained diffuse but the characteristics of the frontal zone changed. The portion of the front from north of Lake Erie to central Indiana moved northward and was analyzed as a warm front. The frontal zone from Illinois to Kansas propagated slowly southward. By 0000 GMT 11 May the frontal zone in Ohio ceased moving northward and assumed the characteristics of a cold front accelerating to the east, with severe weather located ahead of the front in Ohio.

The convective storms began developing in eastern Indiana and northwest Ohio ahead of the front by 1740 GMT and rapidly evolved into several squall lines which propagated eastward during the afternoon (Fig. 9). A separate squall line developed in southern Illinois—southeast Missouri and propagated to the Kentucky—Tennessee border by 2340 GMT in association with the front extending into Missouri. The storms in Indiana and Ohio were responsible for 9 confirmed tornados and 15 funnel cloud reports, while the southern system produced 5 confirmed tornados and 6 funnel clouds.

b. Upper air analyses

The upper air analyses in this study are subjective. The isentropic and pressure surface analyses are cross checked with 15 vertical cross sections to incorporate the detailed vertical resolution of individual rawinsonde ascents into the wind, pressure and moisture analyses on isentropic surfaces and wind, temperature and moisture analyses on pressure surfaces (see Shapiro, 1970; Fig. 2). The cross-check technique also insures consistency between analyses on pressure and isentropic surfaces for each time period.

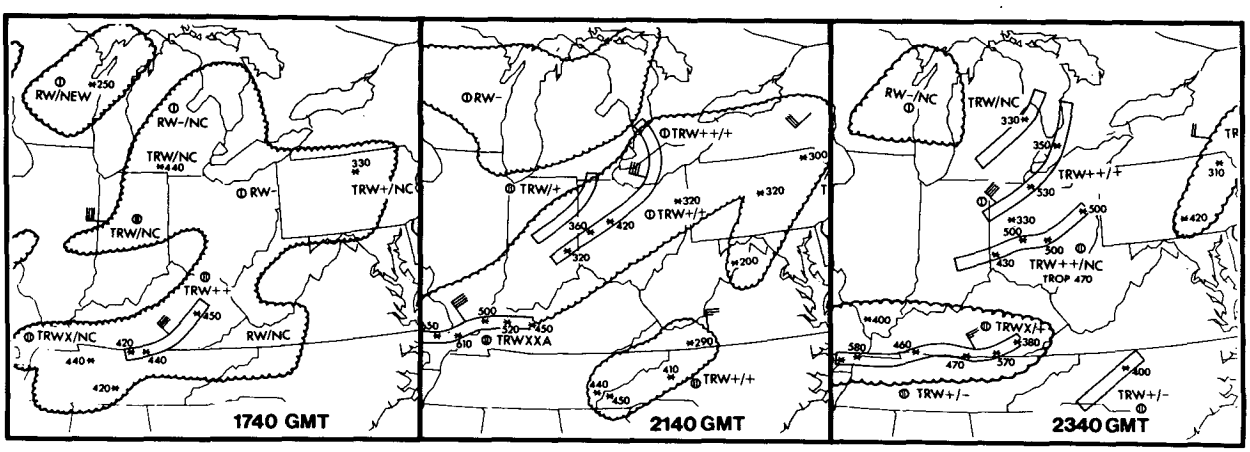

FIG. 9. Radar depictions, 10 May 1973. Cloud tops in hundreds of feet (430 = 43000 ft), RW rainshowers, TRW thundershowers.

At 1200 GMT 10 May, three jet streaks on the 330 K surface (Fig. 10A) were embedded within a general westerly flow stretching from the West Coast to the Great Lakes region. Of primary interest is the upper tropospheric jet streak with a maximum wind speed slightly over 60 m s^{-1} extending from Nebraska to Iowa. The isotach analysis on the 300 K surface (Fig. 10B) illustrates general westerly flow with no evidence of a LLJ perpendicular to the axis of the upper tropospheric jets at this time. The 850 mb isotach analysis for 1200 GMT 10 May (not shown) did indicate that relatively weak, south to southwest winds on the order of 5 m s^{-1} existed over west central Illinois. An extensive band of moisture with mix-

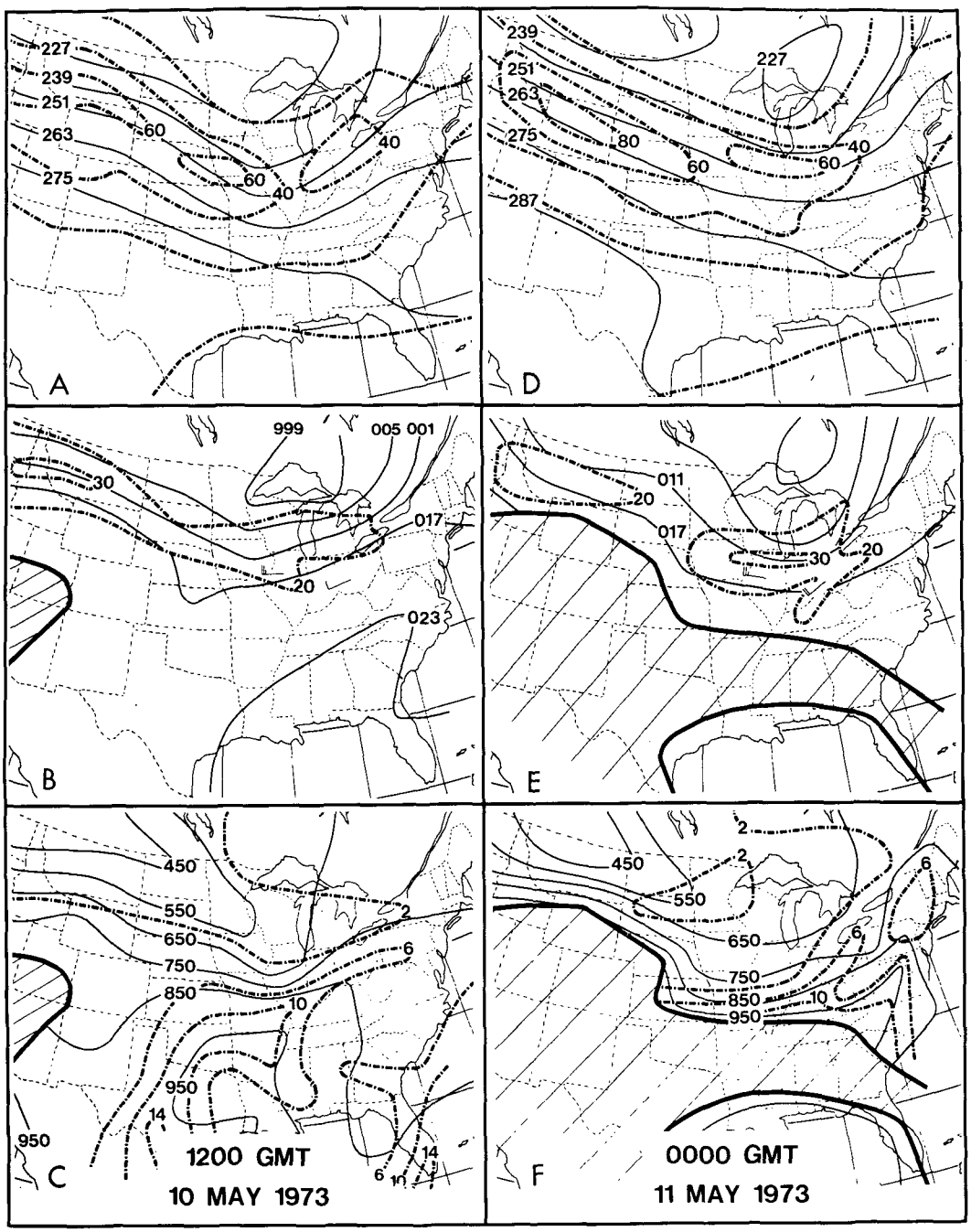

FIG. 10. Isentropic analyses for 1200 GMT 10 May and 0000 GMT 11 May 1973. (A), (D) 330 K isotach and ψ; (B), (E) 300 K isotach and ψ, with isotachs (dashed, m s^{-1}) and ψ (solid, 275 = 3.275 × 10^5 m^2 s^{-2}); (C), (F) 300 K pressure (solid, mb) and moisture (dashed, g kg^{-1}).

ing ratios exceeding 6 g kg^{-1} extended northward from the Gulf of Mexico into the Central Plains and then eastward into southwestern Pennsylvania (Fig. 10C). The moisture tongue from southern Illinois to Pennsylvania was parallel to the isobars (a measure of the slope of the 300 K surface) and generally remained below the 800 mb level.

By 0000 GMT 11 May, the jet streak over the Central Plains intensified slightly and propagated eastward, extending from eastern Iowa to northwest Ohio (Fig. 10D). At the same time a low-level jet with southwesterly winds >20 m s^{-1} existed on the 300 K surface and extended from the 950 mb level in northern Kentucky to 700 mb in western Pennsylvania (Fig. 10E). The moisture tongue sharpened considerably by 0000 GMT, stretched from Kentucky to Ohio coincident with the axis of the LLJ, and was directed up the isentropic surface to the 700 mb level in northeast Ohio (Fig. 10F). Another wind maximum >30 m s^{-1}, as supported by information gained by cross-section analysis, is also evident on the 300 K surface in northern Illinois (Fig. 10E) and apparently represents the downward extension of the upper tropospheric jet streak analyzed on the 330 K surface. This wind maximum was characterized by a generally westerly flow nearly parallel to the ψ contours and to the 650 mb isobar. The westerly wind maximum was therefore significantly different from the ageostrophic LLJ which accelerated toward the lower ψ values and ascended the 300 K isentropic surface over Ohio.

By 1200 GMT 11 May, the upper tropospheric jet streak, which propagated eastward to Pennsylvania, was orientated more from the southwest to the northeast, had weakened to 45 m s^{-1} and was generally not well defined. On the 300 K surface, both the lower tropospheric wind maximum and moisture tongue broadened considerably, lessened their intensity, and shifted east and south from the 0000 GMT positions.

c. *The lower tropospheric wind maximum at 0000 GMT 11 May*

The development of the LLJ extending from Kentucky to Ohio at 0000 GMT 11 May is the most important feature of this case study. Its relative position on the 850 mb surface (Fig. 11B) within the exit region of the upper tropospheric jet streak at the 300 mb level (Fig. 11A) is nearly identical to Newton's schematic (Fig. 1). While the analysis on the 850 mb pressure surface clearly illustrates the LLJ, the 300 K isentropic analysis (Fig. 10E) better depicts the vertical extent of the LLJ and suggests a direct interaction with the upper tropospheric jet streak analyzed on the 330 K surface. The LLJ was directed up the 300 K isentropic surface, extending from the 950 mb level in Kentucky to 750 mb in Pennsylvania. The LLJ axis was at a noticeable angle to the ψ contours over Ohio and at nearly a 30° angle to the height contours on the 850 mb surface (Fig. 11B), indicating that the wind maximum was significantly ageostrophic and accelerating. With the lower tropospheric wind maximum directed up the sloped isentrophic surfaces and toward the cyclonic side of the upper tropospheric jet streak, it appears that the LLJ was embedded within the return branch of the indirect circulation. It must be emphasized that this lower tropospheric jet streak has different characteristics from the low-level jets common to the southern Great Plains during the spring and summer months (Section 2). The LLJ in this case was maximized in the late afternoon and extended up toward the 700 mb level, unlike the nocturnal jets which at-

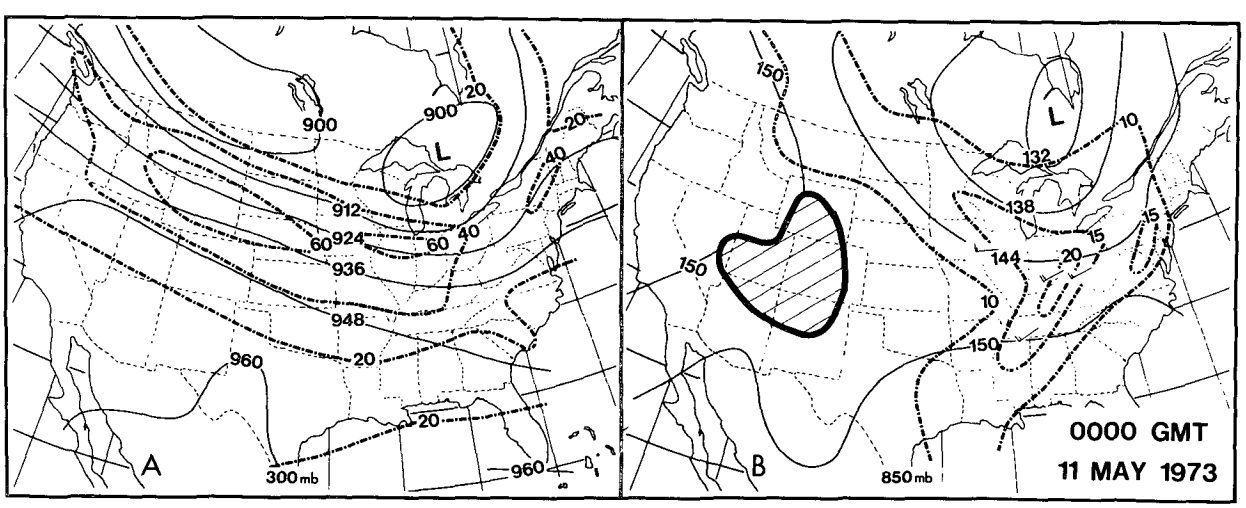

FIG. 11. Pressure surface analyses for 0000 GMT 11 May 1973. (A) 300 mb isotach (dashed, m s^{-1}) and geopotential height (solid, 924 = 9240 m). (B) 850 mb isotachs and geopotential height (solid, 144 = 1440 m).

tain maximum intensity in the early morning and are usually restricted to the planetary boundary layer. The remainder of this case study is concerned with isolating the two-layer mass adjustment associated with the forcing of the return branch and studying the processes responsible for the formation of the LLJ.

d. Analysis of the two-layer mass adjustment

The mass adjustments associated with the jet streak propagating into Ohio at 0000 GMT 11 May are isolated by calculating the tendencies of the hydrostatic pressure difference between isentropic surfaces (Δp) using an overlapping polynomial technique developed by Whittaker and Petersen (1977) and discussed in the Appendix. Fig. 12 illustrates the Δp tendencies within two layers, 340 to 300 K and 300 K to the earth's surface, during the 12 h period (1200 GMT 10 May–0000 GMT 11 May). The pattern of the tendencies for the upper and lower layers is very similar to fields predicted for the jet streak by the hybrid model (Section 3). Within the exit region, upper tropospheric mass convergence and divergence occur on the anticyclonic and cyclonic sides

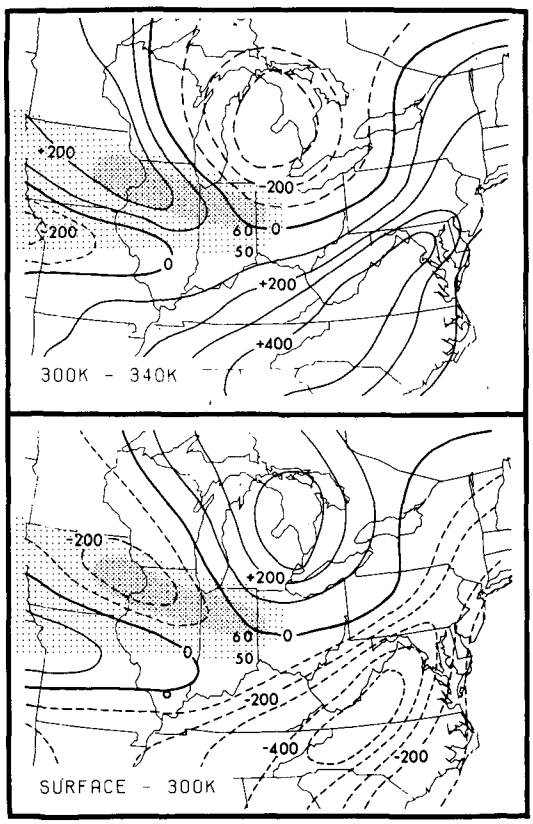

FIG. 12. Mass tendencies ($\times 10^{-1}$ g m^{-2} s^{-1}) for (A) 340 to 300 K layer and (B) from earth's surface to 300 K for period between 1200 GMT 10 May and 0000 GMT 11 May. Light shaded region represents jet streak on 330 K isotachs greater than 50 m s^{-1}; dark shaded region, isotachs greater than 60 m s^{-1} at 0000 GMT 11 May 1973.

yielding the positive and negative tendencies, respectively. The pattern is reversed in the lower layer. Although the mass transports were not explicitly calculated for the diagnostic case study, the two-layer pattern revealed in Fig. 12 is apparently a result of the mass transports associated with the transverse circulations in the exit and entrance regions as simulated by the hybrid model (Section 3).

Supporting evidence of the two-layer mass adjustment ahead of the propagating upper tropospheric jet is illustrated in the vertical cross sections from Sault Ste. Marie, Michigan (SSM) through Ohio to Athens, Georgia (AHN) (Fig. 13). At 1200 GMT 10 May, the mass distribution measured by Δp between the 305 and 325 K isentropic surfaces is relatively uniform along the entire cross section. The jet core located at the 250 mb level between Flint, Michigan (FNT), and Dayton, Ohio (DAY), is identified with the northeastward propagating jet streak centered over southeast Michigan (Fig. 10A). By 0000 GMT 11 May, the jet streak originally located over Nebraska propagated eastward and entered the plane of the vertical cross section near the 375 mb level between FNT and DAY. The mass distribution displays significant changes during this 12 h period with Δp between 305 and 325 K decreasing 200 mb to the left and increasing 150 mb to the right of the streak. The Δp changes in this case replicate the schematic of the two-layer mass adjustment associated with the cross-contour components of the indirect transverse circulations in the exit region (Fig. 7A and 7B). However, the change in Δp in the lower layer to the right of the jet could also be related to diabatic fluxes associated with planetary boundary layer processes and latent heat release (Figs. 7C and 7D).

e. The lower tropospheric isallobaric wind

The impact of the two-layer mass adjustment on the isallobaric wind is determined through an evaluation of (9) and (10) for the 300 K surface. The analysis of the integrated pressure tendency term in (9) is presented in Fig. 14. A four-cell pattern is apparent with the integrated pressure tendency increasing to the right and decreasing to the left of the jet streak in the exit region. In the entrance region a weaker reversed cross-stream variation of the integrated pressure tendency is present. The cross-stream variation of the integrated pressure tendencies is forced by the two-layer mass adjustment. In the exit region, mass convergence above 300 K and mass divergence below forced the 300 K surface to higher pressure on the anticyclonic side. On the cyclonic side, the reversed pattern forced the 300 K surface to lower pressure. In the entrance region, the opposite pattern of the integrated pressure tendencies indicates a reversed two-layer adjustment.

The influence of the integrated and surface pressure tendency terms on the 300 K isallobaric wind as

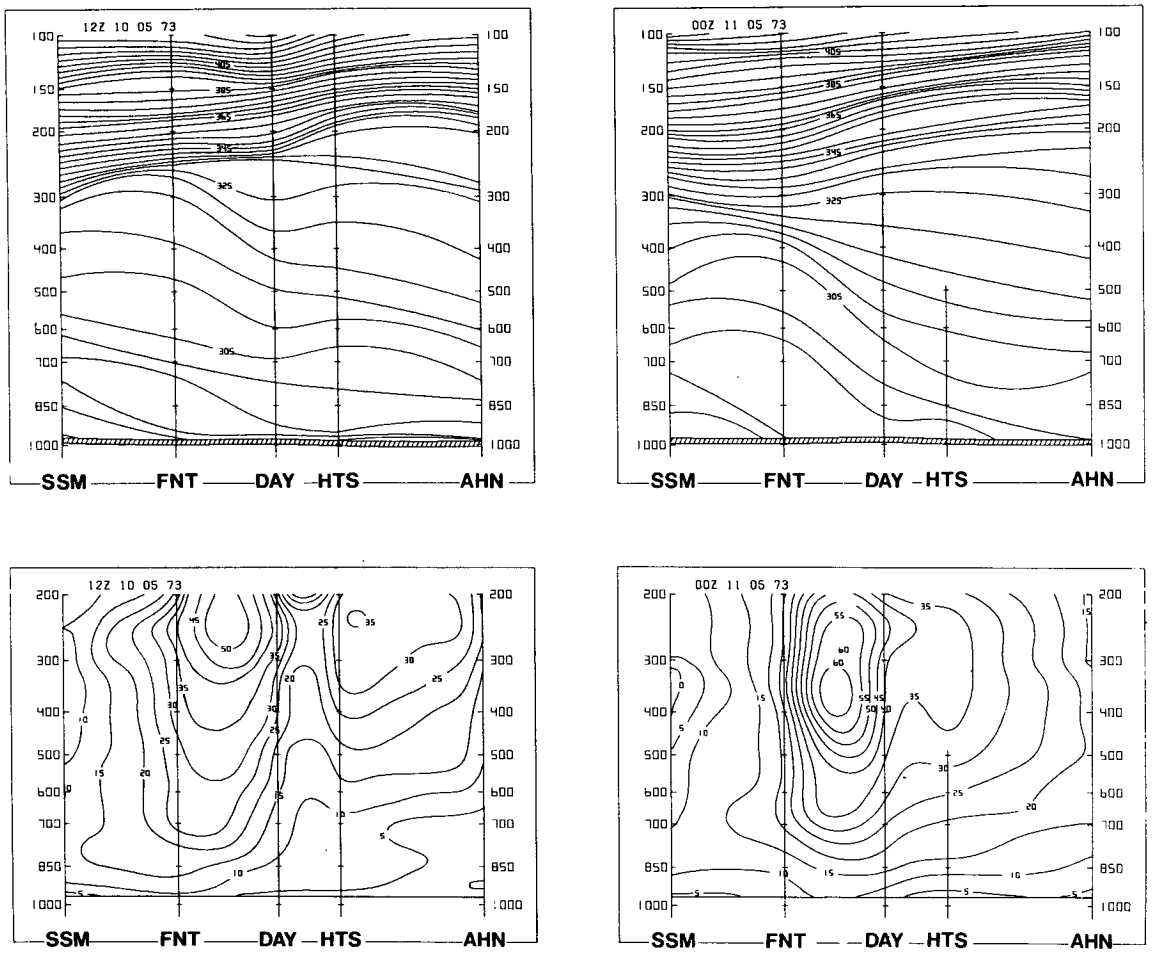

FIG. 13. Vertical cross sections (1200 GMT 10 May 1973 left, 0000 GMT 11 May 1973 right). Potential temperatures (K) top and isotachs (m s^{-1}) bottom.

specified by (10) is presented in Fig. 15. The isallobaric wind vectors (Fig. 15A) converged toward the cyclonic wave in Michigan and toward the mean frontal position through western Ohio and Kentucky (Fig. 8). The maximum isallobaric wind vectors from southern Wisconsin to northeast Indiana are above the 650 mb level and reflect the deepening mid-tropospheric wave in the Great Lakes region. The isallobaric wind beneath the exit region of the upper tropospheric jet streak was orthogonal to the axis of the streak and directed toward the cyclonic side. This ageostrophic component represents the lower branch of the indirect circulation that was evident in the numerical simulation (Section 3).

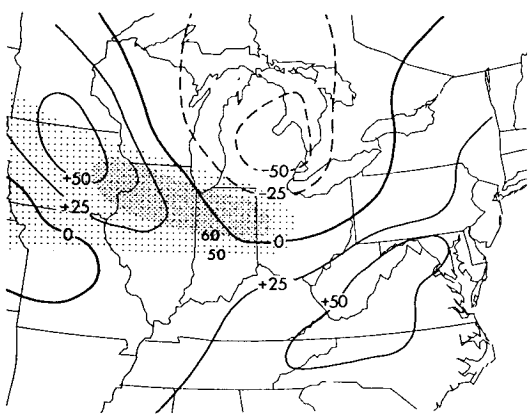

FIG. 14. Integrated pressure tendency term [Eq. (9)] with θ_L = 300 K for period between 1200 GMT 10 May and 0000 GMT 11 May ($\times 10^{-4}$ m^2 s^{-3}). See caption for Fig. 12 for additional details.

The southerly isallobaric wind within the lower branch of the indirect circulation in north central Ohio is of particular interest since it coincides with the position of the LLJ over Ohio at 0000 GMT 11 May. The isallobaric wind component in this region was dominated by the integrated pressure tendency term (Fig. 15B) over the surface pressure tendency term (Fig. 15C). The positive integrated pressure tendency to the right of the jet in the exit region and negative tendency to the left (Fig. 14) was forced by the internal two-layer mass adjustment within the exit region.

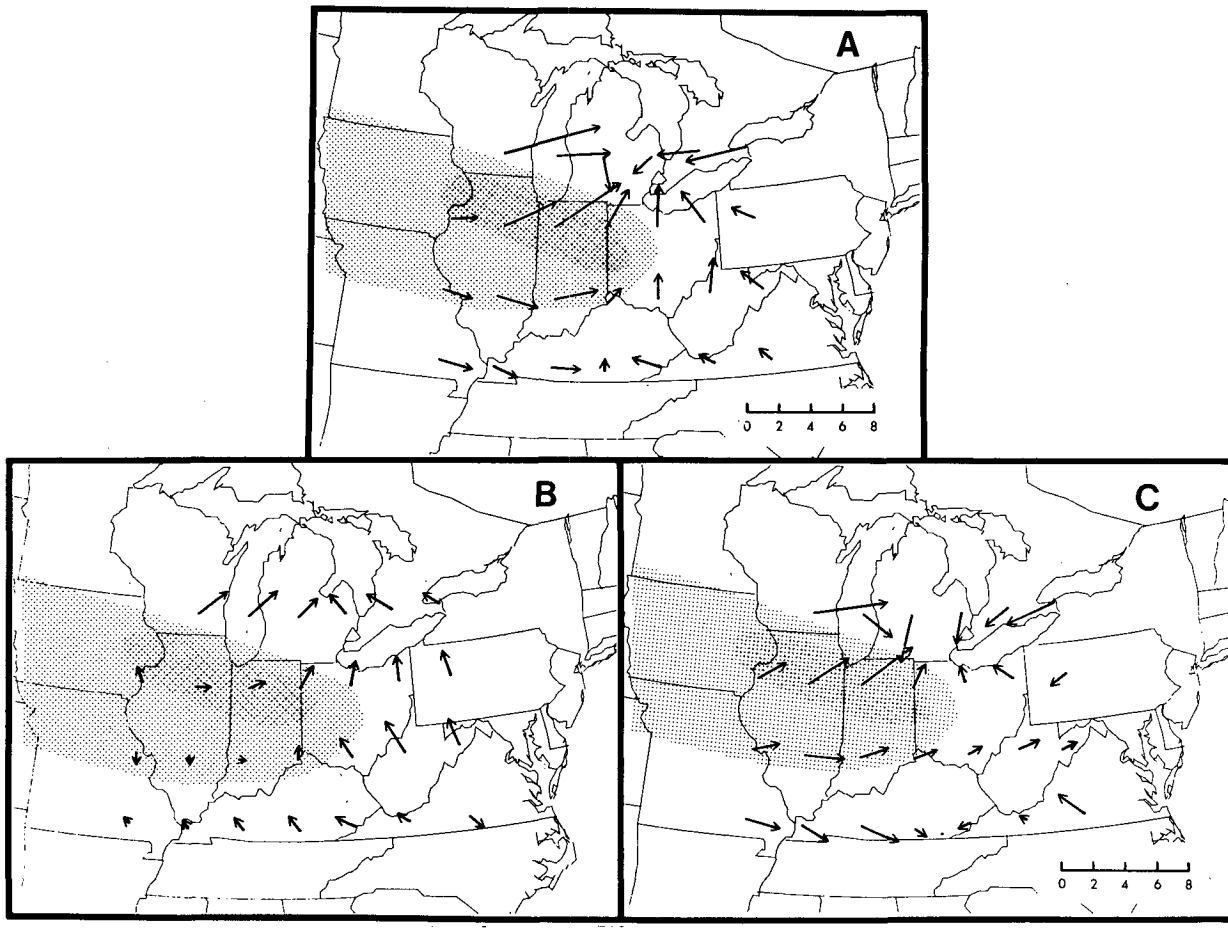

FIG. 15. Evaluation of isallobaric wind [Eq. (10)] and contributing terms for 12 h period 1200 GMT 10 May to 0000 GMT 11 May 1973: (A) vector representation for negative tendency of pressure gradient force [multiplication by f^{-2} yields isallobaric wind], (B) negative integrated pressure tendency term, (C) negative surface pressure tendency term. Magnitude is scaled to lower right of each figure ($\times 10^{-8}$ m s^{-3}). Shaded region represents jet streak at 0000 GMT 11 May, see Fig. 12 for details.

f. A diagnostic trajectory analysis

Trajectories were computed and geostrophic and ageostrophic components of the wind were analyzed to determine the impact of the isallobaric wind on the development of the LLJ. The trajectories are calculated by a diagnostic technique that is based on Greenspan's (1972, 1973) discrete model formulation and which utilizes the primitive form of the inviscid equations of motion (Petersen and Uccellini, 1979). The success of this trajectory technique, like others, is susceptible to analysis errors and violation of the assumptions. However, it should be emphasized that the discrete model approach nearly conserves energy (Petersen and Uccellini, 1979) and that the trajectories represent an accurate response to the calculated ψ tendencies insofar as the inviscid and adiabatic assumptions are satisfied. The final parcel velocities were compared to the subjective isotach analysis for 0000 GMT 11 May to check the accuracy of the trajectory computations and were generally within 3 m s^{-1} and 20° of the subjective isotach and isogon analyses from 0000 GMT 11 May.

Six trajectories on the 300 K surface that were selected from over 40 trajectories calculated by the discrete model approach are illustrated in Fig. 16. Trajectories A and D depict the parcel movement through the lower extension of the upper tropospheric jet streak located at approximately the 650 mb level. The acceleration of parcel D to 30 m s^{-1} over northern Indiana agrees with the observed winds at 0000 GMT 11 May (Fig. 10E). Trajectories C, E and F illustrate the parcels that originate in the lower troposphere and accelerate northeastward through Ohio and toward Pennsylvania. The parcels entering southern Ohio turn toward the north and accelerate up the isentropic surface (toward lower pressure) in the region where the southerly isallobaric wind component was the largest (Fig. 15A) and where the LLJ existed at 0000 GMT 11 May (Fig. 10E). Parcels C and E, for example, accelerated to wind speeds of 23 and 18 m s^{-1} between 1800 and 0000

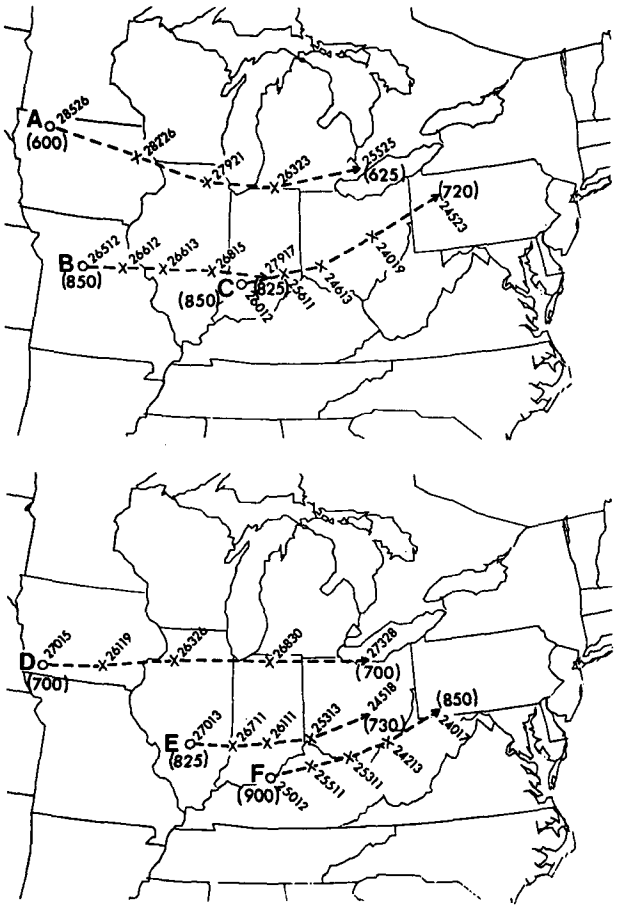

FIG. 16. Parcel trajectories calculated on 300 K isentropic surface for the 12 h period 1200 GMT 10 May to 0000 GMT 11 May 1973; wind velocity is indicated at 3 h positions (24017 is 240° at 17 m s^{-1}); initial and final pressures (mb) are indicated in parentheses.

GMT, respectively, and ascended from below 825 mb to above the 750 mb level. The upward vertical motion indicated by these parcel trajectories reflects the increasing slope of the 300 K surface and the southerly wind component directed toward lower pressure on the 300 K surface (Figs. 10C, 10E and 10F).

The total, geostrophic and ageostrophic wind components and the isallobaric ageostrophic components for parcels C, E and D are presented in Table 1. The geostrophic and isallobaric winds were determined by specifying grid-point ψ values and ψ tendencies for each time by the overlapping polynomial technique (Appendix), calculating geostrophic and isallobaric wind components at the grid points and interpolating to the parcel position. The ageostrophic wind is calculated from the difference between the total and geostrophic winds.

Parcels C and E were chosen since their trajectories pass through the region in which the LLJ formed by 0000 GMT 11 May. The total u and v wind components for C increased 4.6 and 4.4 m s^{-1}, respectively, as it moved into central Ohio at 2100 GMT. Parcel E underwent a similar acceleration as it entered central Ohio at 0000 GMT 11 May. The increases in the v component for C and E are largely due to the increases in v_{ag}. For parcel C, v_{ag} increased to 4.1 m s^{-1} in central Ohio by 2100 GMT and for E to 4.6 m s^{-1} by 0000 GMT. The intensification of v_{ag} is to a large degree accounted for by the increase of the isallobaric v component to 3.0 m s^{-1}. The increase in v_{ag} as parcels C and E entered Ohio is responsible for the computed acceleration of the u component through inertial rotation. The increases in u_g as parcels C and E entered Ohio is consistent with the strengthening north–south ψ gradient on the 300 K surface in that region.

TABLE 1. Total, geostrophic, ageostrophic and isallobaric wind components for parcel trajectories C, E, D in Fig. 17.

Hour	Position	Parcel velocity	u	v	u_g	v_g	u_{ag}	v_{ag}	u_{ag_i}	v_{ag_i}
				Parcel C						
1200 GMT	SW Indiana	260 12	11.8	2.0	10.0	3.2	1.8	−1.2	0.5	0.0
1800 GMT	SW Ohio	246 13	11.9	5.2	13.0	4.0	−1.1	1.2	0.0	2.0
2100 GMT	E central Ohio	240 19	16.5	9.6	16.5	5.5	0.0	4.1	−0.3	3.0
0000 GMT	NW Pennsylvania	245 23	20.8	9.7	16.5	8.0	4.3	1.7	−0.5	1.3
				Parcel E						
1200 GMT	S Illinois	270 13	13.0	0.0	14.5	3.1	−1.5	−3.1	0.9	−0.5
1800 GMT	S central Indiana	261 11	10.8	1.7	10.5	1.2	0.3	0.5	1.0	0.0
2100 GMT	SW Ohio	253 13	12.4	3.8	14.0	1.5	−1.6	2.3	1.0	2.0
0000 GMT	S central Ohio	245 18	16.3	7.6	18.0	3.0	−1.7	4.6	0.7	3.0
				Parcel D						
1200 GMT	SW Iowa	270 15	15.0	0.0	—	—	—	—	—	—
1800 GMT	N Illinois	263 26	25.8	3.1	22.0	0.0	3.8	3.1	3.0	1.5
2100 GMT	N Indiana	268 30	29.9	1.0	25.5	−1.0	4.4	2.0	2.0	2.0
0000 GMT	N Ohio	273 28	27.9	−1.5	24.0	5.0	3.9	−6.5	−0.7	1.7

Parcel D illustrates the response of super-geostrophic parcels entering northern Ohio upon exiting the lower extension of the upper tropospheric jet streak. As D entered northern Ohio (0000 GMT), it turned slightly to the south with the v_{ag} decreasing from 2.0 to -6.5 m s^{-1}. The negative v_{ag} depicts the response of D after movement through the jet streak in northern Indiana into a region of a weaker pressure gradient force and indicates that for supergeostrophic parcels exiting the streak, the inertial effect [term B in Eq. (3)] dominates the positive isallobaric contribution in northern Indiana and Ohio. Comparing supergeostrophic parcel D with the initially subgeostrophic parcels C and E shows that the isallobaric component dominates the ageostrophic wind in the lower troposphere to the south and southwest, while the inertial component dominates the middle troposphere to the west and northwest. The patterns of motion and acceleration for these trajectories from the northwest and southwest infer deformation and/or convergence in the vicinity of the front near which the severe weather developed.

The analysis of the trajectories indicates that the increases in the u and v components for lower tropospheric parcels entering the region of the LLJ over southwest Ohio are consistent with the expected response of the lower tropospheric wind to the mass adjustments in the exit region of an upper tropospheric jet streak and the increasing pressure gradient force on lower tropospheric isentropic surfaces. The isallobaric component associated with the increased pressure gradient force accounts for over half of the increase in the southerly ageostrophic wind in Ohio. The southerly ageostrophic wind forces a corresponding increase in the u component through inertial rotation. The result of the increases in the v_{ag} and u components is the formation of the LLJ directed toward the northeast, oriented at a significant angle to the axis of the upper tropospheric jet streak (Fig. 11).

g. Implications of coupled jet streaks for convective storm development

The impact of the coupled jets on creating conditions favorable for the deep convection in this case study was determined by computing the meridional moisture and sensible heat transports along a cross section from southern New York westward to Nebraska (Fig. 17). With the large increase of the lower tropospheric meridional component associated with the development of the LLJ, the maximum northward moisture transport over Ohio increased from 30 to 102 g m^{-2} s^{-1}, or an equivalent increase in the transport of latent energy from 7.6 to 25.7 $\times$ 10^4*J* m^{-2} s^{-1} and lowered to the layer within which the LLJ formed (Fig. 17B). For the same 12 h period, the maximum northward sensible heat transport over Ohio increased from 12.6 to 28.1 $\times$ 10^5*J* m^{-2} s^{-1} in conjunction with the development of the LLJ.

The impact of the increased southerly wind in the lower troposphere and at the earth's surface in the region where the LLJ developed is also illustrated by the surface equivalent potential temperature (θ_e) analyses (Fig. 18). The θ_e analyses are based on hourly surface data from nearly 100 Midwest reporting stations. The increased temporal and spatial resolution lend valuable supporting evidence to the interpretation that the LLJ increased the lower tropospheric moisture and heat transports into the inception area of the severe convective storms. A θ_e tongue rapidly intensified and, by 1800 GMT 10 May, extended northeastward into Ohio coinciding with the axis of the LLJ at 0000 GMT 11 May. Although the daytime insolation can significantly increase the surface θ_e, the increase by insolation would tend to be uniform at any given latitude. The shape and preferred location of the narrow θ_e tongue coinciding with the axis of the LLJ points to the importance of the accelerated advective process in the rapid evolution of the θ_e field in southeastern Indiana and western Ohio. As in other cases (Means, 1952, 1954; Bonner, 1966), the narrow region of accelerated moisture and temperature advections in the boundary layer is due to the increased lower tropospheric winds associated with the development of the LLJ.

While the development of the LLJ increased the lower tropospheric θ_e in Ohio by rapid northward transport of sensible heat and moisture, the lower portion of the upper tropospheric jet streak that extended down to the 600–700 mb layer (see 300 K analysis, Fig. 10E) transported cooler and drier air into the middle troposphere. The effect of the differential transports was to reduce θ_e by about 4 K within the 500 to 750 mb layer for the Dayton, Ohio soundings from 1200 GMT 10 May to 0000 GMT 11 May, while lower tropospheric θ_e values increased by 4 to 12 K. By 0000 GMT 11 May, the Dayton sounding indicated convective instability from the earth's surface to 500 mb, and that the level of free convection was lowered from 770 to 850 mb, while the equilibrium level at the top of the positive energy area of latent instability increased from 680 to 270 mb. The net effect of the differential sensible heat and moisture transports associated with the coupled jet streaks was to create conditions favorable for the formation of deep convective storms that developed within the exit region of the upper tropospheric jet streak by 0000 GMT.

5. Summary

The interaction between upper and lower tropospheric jet streaks is an important factor in the development of organized severe convective storm systems. The intersection of jet axes in the exit re-

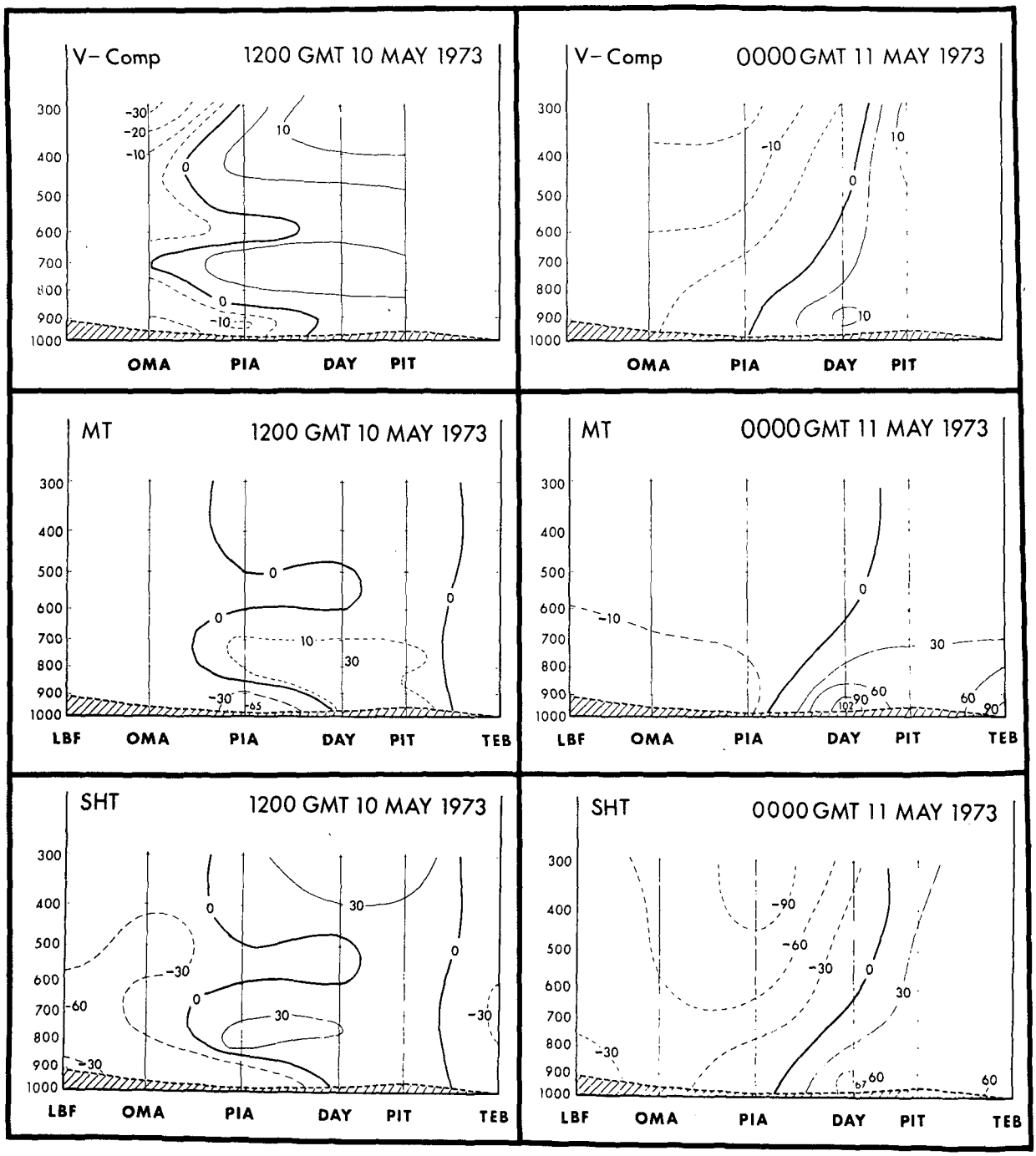

FIG. 17. Vertical cross sections of (A) meridional wind component (m s^{-1}) from Omaha, Nebraska (OMA) to Pittsburgh, Pennsylvania (PIT); (B) meridional moisture transport (MT, g m^{-2} s^{-1}) and sensible heat transport (SHT, $\times 4.2 \times 10^4 J$ m^{-2} s^{-1}) from North Platte, Nebraska (LBF) to Teterboro, New Jersey (TEB). Northward directed fluxes are positive (solid), southerly fluxes are negative (dashed).

gion of the upper tropospheric jet and the veering of the wind with height convectively destabilizes the atmosphere through differential moisture and temperature advections (Miller, 1955; Petterssen, 1956; Newton, 1967). In most studies, the tendency has been to treat each jet streak as a separate entity, although Reiter (1969) suggested that in some cases upper and lower tropospheric jet streaks are not separate entities. This paper has presented a basis for the dynamical processes responsible for coupling upper and lower tropospheric jet streaks through mutual mass-momentum adjustments and transverse

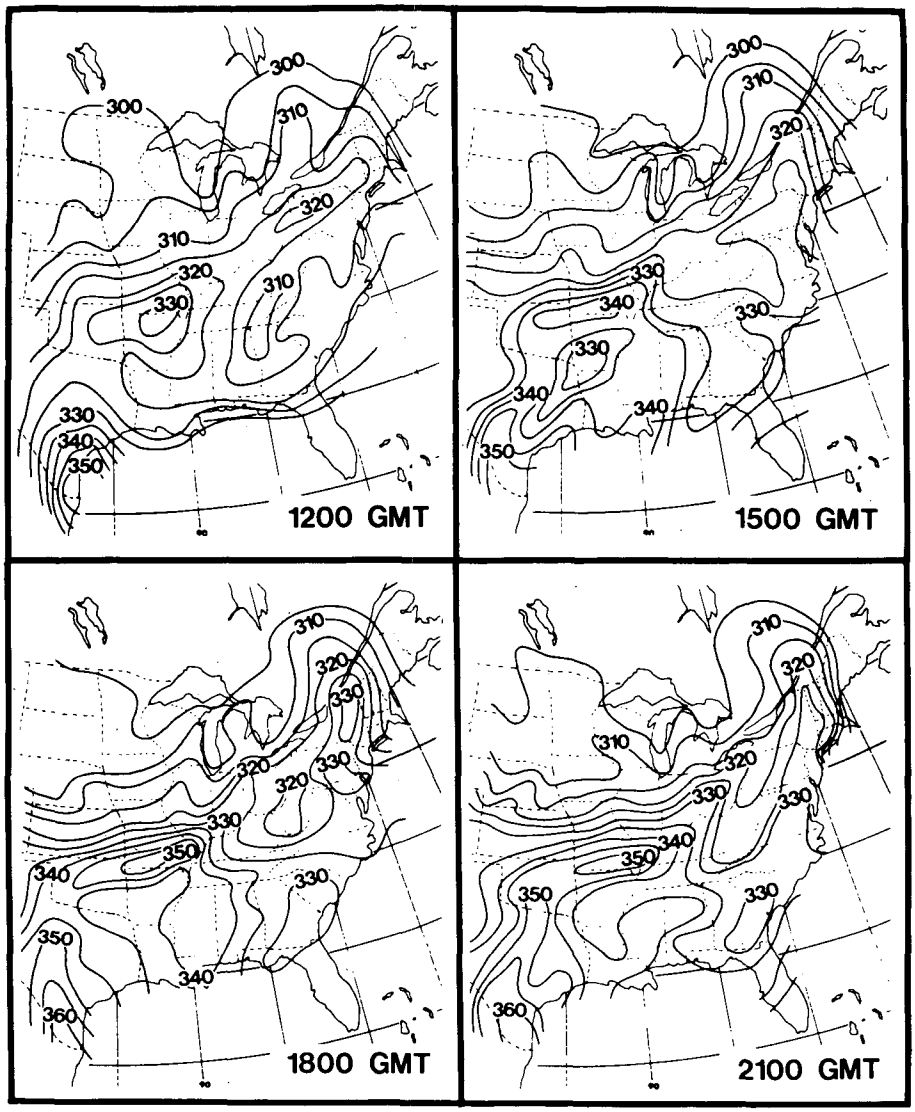

FIG. 18. Surface equivalent potential temperature (θ_e) analyses for 10 May 1973, based on FAA and Weather Service hourly surface data.

circulations within the exit region of an upper level jet streak. The forcing of the transverse circulations was investigated by the combined application of the geostrophic momentum approximation and isallobaric equation in isentropic coordinates.

A hybrid numerical model is used to simulate the mass adjustment associated with a jet streak propagating in a zonal channel and the response of the lower troposphere. The model simulation depicts a basic two-layer mass adjustment in the exit and entrance regions of the jet streak that was related primarily to the ageostrophic mode. At the level of the jet streak, the inertial advective component of the geostrophic momentum approximation to the ageostrophic wind dominated the upper branches of the transverse circulations. In the lower troposphere, the isallobaric component of the ageostrophic wind dominated the lower branch of the transverse circulations. The numerical results verified that the lower tropospheric isallobaric winds, representing the transverse components of the return branches of the direct and indirect circulations, are forced by the two-layer mass adjustment accompanying the propagation of the upper level jet streak.

In the case study, a similar two-layer mass adjustment was isolated in the exit region of the upper tropospheric jet streak and linked to the increased pressure gradient force and the resultant isallobaric component within the return branch of an indirect circulation. The mass adjustment and isallobaric wind were then related to the formation of a low-level jet. The LLJ, located beneath the exit region

of the upper tropospheric jet streak, was embedded within the lower branch of an indirect circulation. The LLJ was directed up sloped isentropic surfaces toward the cyclonic side of the upper level jet and was noticeably ageostrophic. A diagnostic analysis of atmospheric trajectories verifies that a southerly isallobaric wind was an important component of the LLJ in this case. The southerly isallobaric wind was largely responsible for the observed intensification of the meridional ageostrophic wind component and forced a corresponding acceleration of the u component through inertial rotation, while u_g intensified through the increased pressure gradient force. The increases in v_{ag} and u resulted in the formation of the LLJ directed toward the northeast at a significant angle to the axis of the upper tropospheric jet streak. Since the mass adjustments are responsible for the isallobaric ageostrophic wind, the upper tropospheric jet streak and LLJ were coupled by the two-layer mass adjustment associated with the jet streak's propagation. These results, which emphasize momentum generation in the lower troposphere as a result of a three-dimensional mass-momentum adjustment process, are in contrast to Ninomiya's (1971) contention that convection-induced vertical transport of momentum is responsible for the development of a LLJ within the exit region of an upper level jet streak. A downward transport of the upper level jet streak's momentum cannot account for the orthogonal momentum component of the LLJ that yields the difference in wind direction between upper and lower tropospheric jet streaks.

The case study also isolated how the coupling of the upper and lower tropospheric jet streaks yields conditions favorable for the development of severe convective storms within the *exit region* of the *upper tropospheric jet*. The isallobaric wind component of the LLJ that is orthogonal to the axis of the upper tropospheric jet streak was the primary reason for the LLJ being at a significant angle to the jet's axis. The dominance of the isallobaric component in the lower troposphere combined with the increased importance of the inertial advective effects in the middle and upper troposphere resulted in veering of the winds with height and differential moisture and sensible heat transports. The LLJ rapidly transported moisture and sensible heat within the lower troposphere northward into the inception area, while the lower extension of the upper tropospheric jet streak transported cooler and drier air eastward within the middle troposphere. The net effect of the differential transports was to generate convective instability from the earth's surface to the 500 mb level, to lower the level of free convection and to raise the equilibrium level capping latent instability, all of which are conducive to the formation of deep convective storms. The concept that the development of conditions favorable for deep convection occurs through mutual mass-momentum adjustments associated with a propagating jet streak provides an underlying basis for the criteria used in severe weather forecasts (Fawbush *et al.*, 1951; Fawbush and Miller, 1953, 1954).

The primary emphasis of this research has been to determine the role of propagating jet streaks and mass-momentum adjustments in creating conditions favorable for the development of severe convective storm systems. However, several important questions remain for future research. The influence that latent and sensible heating, and subsequent diabatic mass transports, have on the coupling of the lower tropospheric wind response to the propagating upper tropospheric jet streak should be examined through numerical experiments and additional case studies. Another important problem that should be considered in future research is an apparent non-steady aspect of the coupling between upper and lower tropospheric jet streaks. In this case, the sounding data did not indicate a LLJ within the exit region of the upper tropospheric jet streak at 1200 GMT 10 May. Also, the surface θ_e analysis for 1200 GMT did not reveal any distinct θ_e tongues in Illinois and Iowa. The development of a distinct θ_e tongue into southern Indiana and western Ohio during the day (Fig. 18), the reversal of the movement of the frontal zone in that area during the same period (Fig. 8), and the existence of the LLJ at 0000 GMT 11 May suggest that the LLJ did not move with the propagating upper tropospheric jet streak. Rather, the LLJ seemed to develop within the exit region between 1200 GMT 10 May and 0000 GMT 11 May as the upper tropospheric streak approached the surface front extending through Ohio and Indiana. The development of the LLJ appears to represent an acceleration of the transverse indirect circulation with respect to the propagating jet streak. Eliassen (1951) emphasized that the intensity of meridional circulations will increase with reduced stability. In this case, as the upper tropospheric jet streak approached the warmer air east of the front, the jet encountered a region in which the mid-tropospheric stability was significantly reduced on the cyclonic and anticyclonic sides of the streak (indicated by large Δp between 325 and 305 K isentropes in the 1200 GMT vertical cross section in Fig. 13). Perhaps the reduced stability in the region into which a jet streak propagates is a key factor for the intensification of the indirect circulation and a subsequent increase in the magnitude of the low-level winds. The examination of these questions could provide additional insight into the scale interactive processes that establish convective instability and initiate and maintain the severe convective storm systems.

Acknowledgments. We express our appreciation to Drs. J. A. Young, W. Schwerdtfeger and L. H.

Horn for their useful comments during the course of this research. We thank the reviewers for their valuable comments which helped to clarify portions of the manuscript. We also thank Thomas M. Whittaker for assisting in the computer programming, Jim Vergin and Jack Katzfey for assisting in data analysis and John Stremikis, Jean Johnson and Nancy Malz for preparing the manuscript. This research was sponsored by the Atmospheric Science Section, National Science Foundation, under Grants ATM75-23223 and ATM77-22976.

APPENDIX

The Calculation of the Isallobaric Wind and Mass Tendencies for the Case Study

The ψ and pressure tendencies in (11) and (12) are evaluated utilizing the "overlapping polynomial technique" developed by Bleck and Haagenson (1968) and expanded on by Whittaker and Petersen (1977). The method was designed for spatial objective analyses but can also be used to generate temporal series. In an example from Whittaker and Petersen (see Whittaker and Petersen, 1977; Fig. 3), two second-order polynomials are fitted between four data points. In the region between the second and third points, the two curves are merged using linear distance weighting to yield the resultant third-order polynomial. The method maintains a smooth transition between adjacent polynomials and insures that first derivatives can be calculated along the entire curve. In our application, the four data points represent sounding data from 0000 GMT 10 May through 1200 GMT 11 May 1973 at 12 h intervals. The period of interest in this case study is between the second and third points, 1200 GMT 10 May and 0000 GMT 11 May, respectively. This technique is utilized to generate time series which are then used 1) to calculate the pressure at the midpoint of the series (1800 GMT 10 May) at each grid point for estimating the two contributing terms to $\mathbf{U}_{ag_i}$ in (10); 2) to specify the ψ tendencies in the trajectory analysis; and 3) to calculate the isallobaric component for parcel trajectories in Table 1 by computing grid-point tendencies of pressure gradient force at 3 h intervals with Δt set equal to 2 h, which are then interpolated to the parcel positions.

REFERENCES

Beebe, R. G., and F. C. Bates, 1955: A mechanism for assisting in the release of convective instability. *Mon. Wea. Rev.*, **83**, 1–10.

Bjerknes, J., 1951: Extratropical cyclones. *Compendium of Meteorology*, T. F. Malone, Ed. Amer. Meteor. Soc., 577–598.

Blackadar, A. K., 1957: Boundary layer wind maxima and their significance for the growth of nocturnal inversions. *Bull. Amer. Meteor. Soc.*, **38**, 283–290.

Bleck, R., and P. L. Haagenson, 1968: Objective analysis on isentropic surfaces. NCAR Tech. Note, NCAR-TN-39, 27 pp.

Bonner, W. D., 1966: Case study of thunderstorm activity in relation to the low-level jet. *Mon. Wea. Rev.*, **94**, 167–178.

——, 1968: Climatology of the low level jet. *Mon. Wea. Rev.*, **96**, 833–850.

Browning, K. A., and T. W. Harrold, 1970: Air motion and precipitation growth at a cold front. *Quart. J. Roy. Meteor. Soc.*, **96**, 369–389.

Brunt, D., and C. K. M. Douglas, 1928: *Memo. Roy. Meteor. Soc.*, **3**, No. 22.

Cahir, J. J., 1971: Implications of circulations in the vicinity of jet streaks at subsynoptic scales. Ph.D. thesis, Pennsylvania State University, 170 pp.

Cahn, A., 1945: An investigation of the free oscillations of a simple current system. *J. Meteor.*, **2**, 113–119.

Danielsen, E. F., 1974: The relationship between severe weather, major dust storms and rapid cyclogenesis. *Synoptic Extratropical Weather Systems*, M. Shapiro, Ed., National Center for Atmospheric Research, 215–241.

Eliassen, A., 1949: The quasi-static equations of motion with pressure as independent variable. *Geofys. Publ.*, **17**, 5–44.

——, 1951: Slow thermally or frictionally controlled meridional circulation in a circular vortex. *Astrophy. Norv.*, **5**, 19–60.

——, 1962: On the vertical circulation in frontal zones. *Geofys. Publ.*, **24**, 147–160.

Fawbush, E. J., and R. C. Miller, 1953: The tornado situation of 17 March 1951. *Bull. Amer. Meteor. Soc.*, **34**, 139–145.

——, and ——, 1954: The types of air masses in which North American tornadoes form. *Bull. Amer. Meteor. Soc.*, **35**, 154–165.

——, —— and L. G. Starrett, 1951: An empirical method of forecasting tornado development. *Bull. Amer. Meteor. Soc.*, **32**, 1–9.

Gerhardt, J. R., 1962: An example of a nocturnal low-level jet stream. *J. Atmos. Sci.*, **19**, 116–118.

——, 1963: Mesoscale association of a low-level jet stream with a squall-like cold-front situation. *J. Atmos. Sci.*, **20**, 49–55.

Greenspan, D., 1972: A new explicit discrete mechanics with applications. *J. Franklin Inst.*, **294**, 231–240.

——, 1973: *Discrete Models*. Addison-Wesley, 105–107.

Hess, S. L., 1959: *Introduction to Theoretical Meteorology*. Holt, Rinehart and Winston, 225–227.

Hoecker, W. H., 1963: Three southerly low-level jet streams delineated by the Weather Bureau special pibal network of 1961. *Mon. Wea. Rev.*, **91**, 573–582.

Hoskins, B. J., 1975: The geostrophic momentum approximation and the semi-geostrophic equations. *J. Atmos. Sci.*, **32**, 233–242.

Izumi, Y., 1964: The evolution of temperature and velocity profiles during breakdown of a nocturnal inversion and a low-level jet. *J. Appl. Meteor.*, **3**, 70–82.

——, and M. L. Barad, 1963: Wind and temperature variations during development of a low-level jet. *J. Appl. Meteor.*, **2**, 668–673.

Johnson, D. R., 1970: The available potential energy of storms. *J. Atmos. Sci.*, **27**, 727–741.

Lettau, H. H., 1967: Small to large scale features of boundary structures over mountain slopes. *Proc. Symp. Mountain Meteor.*, Colorado State University, 1–74.

Ludlam, F. H., 1963: *Severe Local Storms: A Review. Meteor. Monogr.*, No. 27, Amer. Meteor. Soc., 1–30.

Means, L. L., 1952: On thunderstorm forecasting in the central United States. *Mon. Wea. Rev.*, **80**, 165–189.

——, 1954: A study of the mean southerly wind maxima in low levels associated with a period of summer precipitation in the middle west. *Bull. Amer. Meteor. Soc.*, **35**, 166–170.

Miller, J. E., 1955: Intensification of precipitation by differential advection. *J. Meteor.*, **12**, 472–477.

Murray, R., and S. M. Daniels, 1953: Transverse flow at entrance and exit to jet streams. *Quart. J. Roy. Meteor. Soc.*, **79**, 236–241.

Namias, J., and P. F. Clapp, 1949: Confluence theory of the high tropospheric jet stream. *J. Meteor.*, **6**, 330–336.

Newton, C. W., 1954: Frontogenesis and frontolysis as a three-dimensional process. *J. Meteor.*, **11**, 449–461.

——, 1959: Axial velocity streaks in the jet stream: ageostrophic "inertial" oscillations. *J. Meteor.*, **16**, 638–645.

——, 1963: Dynamics of severe convective storms. *Meteor. Monogr.*, No. 27, Amer. Meteor. Soc., 33–55.

——, 1967: Severe convective storms. *Advances in Geophysics*, Vol. 12, Academic Press, 257–303.

Ninomiya, K., 1971: Mesoscale modification of synoptic situations from thunderstorm development as revealed by ATS III and aerological data. *J. Appl. Meteor.*, **10**, 1103–1121.

Paegle, J., and G. E. Rasch. 1973: Three-dimensional characteristics of diurnally varying boundary-layer flows. *Mon. Wea. Rev.*, **101**, 746–756.

Palmén, E., and C. W. Newton, 1969: *Atmospheric Circulation Systems*. Academic Press (see Chaps. 4, 5, 8, 9 and 13).

Petersen, R. A., and L. W. Uccellini, 1979: The computation of isentropic atmospheric trajectories using a "discrete model" approach. *Mon. Wea. Rev.*, **107**, 566–574.

Petterssen, S., 1956: *Weather Analysis and Forecasting*, Vol. 2. McGraw-Hill, 191–195.

Reiter, E. R., 1963: *Jet-Stream Meteorology*. The University of Chicago Press (see Chaps. 4 and 6).

——, 1969: Tropopause circulation and jet streams. *World Survey of Climatology*, Vol. 4., *Climate of the Free Atmosphere*, D. F. Rex, Ed., 85–193.

Riehl, H., et al., 1952: *Forecasting in the Middle Latitudes. Meteor. Monogr.*, No. 5, Amer. Meteor. Soc., 80 pp.

Rossby, C. G., 1938: On the mutual adjustment of pressure and velocity distributions in certain simple current systems II. *J. Mar. Res.*, **7**, 239–263.

——, 1949: On the nature of the general circulation of the lower atmosphere. *The Atmosphere of the Earth and Planets*, G. P. Kuiper, Ed., The University of Chicago Press, 16–48.

Sawyer, J. S., 1956: The vertical circulation at meteorological fronts and its relation to frontogenesis. *Proc. Roy. Soc. London.*, **234A**, 346–362.

Shapiro, M. A., 1970: On the applicability of the geostrophic approximation to upper-level frontal-scale motions. *J. Atmos. Sci.*, **27**, 408–420.

——, 1975: Simulation of upper-level frontogenesis with a 20-level isentropic coordinate primitive equation model. *Mon. Wea. Rev.*, **103**, 591–604.

Staley, D. O., 1960: Evaluation of potential vorticity changes near the tropopause and the related vertical motions, vertical advection of vorticity and transfer of radioactive debris from stratosphere to troposphere. *J. Meteor.*, **17**, 591–620.

Uccellini, L. W., 1976: Operational diagnostic applications of isentropic analysis. *Nat. Wea. Dig.*, **1**, 4–12.

——, D. R. Johnson and R. E. Schlesinger, 1979: An isentropic and sigma coordinate hybrid numerical model: Model development and some initial tests. *J. Atmos. Sci.*, **36**, 390–414.

University of Chicago, 1947: On the general circulation of the atmosphere in middle latitudes. *Bull. Amer. Meteor. Soc.*, **28**, 255–280.

Wexler, H., 1961: A boundary layer interpretation of the low-level jet. *Tellus*, **13**, 368–378.

Whittaker, T. M., and R. A. Petersen, 1977: Objective cross-sectional analysis incorporating thermal enhancement of the observed winds. *Mon. Wea. Rev.*, **105**, 147–153.

Young, J. A., 1973: A theory for isallobaric air flow in the planetary boundary layer. *J. Atmos. Sci.*, **30**, 1584–1592.